



U.S. DEPARTMENT OF
ENERGY

PNNL-20606

Prepared for the U.S. Department of Energy
under Contract DE-AC05-76RL01830

Application of Acoustic Emission and Other Online Monitoring Technologies to High Temperature Gas Reactors

RM Meyer
P Ramuhalli

BG Braatz
SR Doctor

January 2012



Pacific Northwest
NATIONAL LABORATORY

*Proudly Operated by **Battelle** Since 1965*

DISCLAIMER

This report was prepared as an account of work sponsored by an agency of the United States Government. Neither the United States Government nor any agency thereof, nor Battelle Memorial Institute, nor any of their employees, makes **any warranty, express or implied, or assumes any legal liability or responsibility for the accuracy, completeness, or usefulness of any information, apparatus, product, or process disclosed, or represents that its use would not infringe privately owned rights.** Reference herein to any specific commercial product, process, or service by trade name, trademark, manufacturer, or otherwise does not necessarily constitute or imply its endorsement, recommendation, or favoring by the United States Government or any agency thereof, or Battelle Memorial Institute. The views and opinions of authors expressed herein do not necessarily state or reflect those of the United States Government or any agency thereof.

PACIFIC NORTHWEST NATIONAL LABORATORY
operated by
BATTELLE
for the
UNITED STATES DEPARTMENT OF ENERGY
under Contract DE-AC05-76RL01830

Printed in the United States of America

Available to DOE and DOE contractors from the
Office of Scientific and Technical Information,
P.O. Box 62, Oak Ridge, TN 37831-0062;
ph: (865) 576-8401
fax: (865) 576-5728
email: reports@adonis.osti.gov

Available to the public from the National Technical Information Service,
U.S. Department of Commerce, 5285 Port Royal Rd., Springfield, VA 22161
ph: (800) 553-6847
fax: (703) 605-6900
email: orders@ntis.fedworld.gov
online ordering: <http://www.ntis.gov/ordering.htm>



This document was printed on recycled paper.

(9/2003)

Application of Acoustic Emission and Other Online Monitoring Technologies to High Temperature Gas Reactors

RM Meyer
P Ramuhalli

BG Braatz
SR Doctor

January 2012

Prepared for
the U.S. Department of Energy
under Contract DE-AC05-76RL01830

Pacific Northwest National Laboratory
Richland, Washington 99352

Abstract

The Next-Generation Nuclear Plant will be a high temperature gas cooled reactor (HTGR) operating at temperatures up to 950°C and cooled by helium. HTGR designs exist to meet modern demands for safety, modularity, and versatility with respect to the production of electricity, process heat, and hydrogen. While two HTGRs have been licensed and operated in the United States (Fort St. Vrain and Peach Bottom 1), and several more in Europe and Asia, the cumulative operating experience with HTGRs is limited compared to the operating experience accumulated from the operation of Light Water Reactors (LWRs). The minimal operating experience, coupled with the exceptional stress created by the high temperature environment, motivates the application of online monitoring technologies to monitor degradation of structural components. Two online monitoring technologies, Acoustic Emission (AE) and Guided Ultrasonic Waves (GUW), have significant potential for application to HTGRs. This report is an assessment AE and GUW for online monitoring of degradation in HTGRs based on a review of open literature. This literature review was performed through several phases including a literature search, a review of abstracts, selecting and requesting literature that was deemed most relevant, and finally a thorough evaluation of the acquired literature. The literature searches were conducted with the assistance of library staff at Hanford Technical Library. Rules for online degradation monitoring in LWRs with AE are included Section XI and Section V, Article 13 of the ASME Boiler and Pressure Vessel Code. The use of AE for crack monitoring has been demonstrated in the field on operating LWRs. In addition to crack monitoring, AE has been deployed for leak monitoring, and loose parts monitoring. All of these applications are negatively impacted by the presence of background noise in an operating reactor environment. Cavitation is a common source of noise in an LWR environment that is not expected in an HTGR environment. However, an HTGR environment may contain other sources of noise such as cracking and spalling of oxide layers. Higher operating temperatures imply the standoff requirements for sensitive piezoelectric transducers and electronics will be greater in an HTGR environment and may result in decreased sensor sensitivity. Finally, AE has been extensively studied for its ability to detect forms of degradation relevant to LWR materials and environments. Studies investigating the sensitivity of AE to degradation in HTGR environments are limited. GUW is a promising technology and is experiencing increasing interest from the LWR community for application to the inspection of piping and plate-shaped components. GUW holds similar promise for inspecting HTGR components since its long range inspection capability may allow inspection in harsh conditions remotely from a tolerable environment. Additionally, online monitoring of HTGRs with GUW is facilitated by the gas-phase form of the coolant.

Summary

Advanced nuclear power plants, such as the Next-Generation Nuclear Plant, are expected to operate at higher temperatures to take advantage of the higher efficiencies possible in converting thermal energy to electrical energy. Conventional light-water reactors (LWRs) operate at typical efficiencies of 20%–30% (thermal-to-electric), limited primarily by the coolant. High-temperature gas reactors (HTGRs) are a subset of high-temperature reactors, which propose to use a range of coolant materials, including helium or supercritical CO₂ gas, liquid metals (such as liquid sodium), and molten salt to operate at much higher temperatures. HTGR designs are proposed to operate at higher outlet temperatures, on the order of 950°C, which can stress the available materials that are used in the design and construction of the HTGRs. Substantial monitoring and surveillance efforts of structural components are essential to the management of aging and degradation processes in HTGR environments to cope with enhanced material stressors and limited operational experience. In addition, the implementation of on-line refueling (as in the Pebble Bed Modular Reactor) means HTGRs may operate over ten years before encountering a shutdown for fuel management. Ten years is the current inspection interval specified for the inspection of systems, structures, and components in LWRs. Flaw growth rates in HTGRs may be expected to exceed flaw growth rates in LWRs because of higher operating temperatures. To avoid increased frequency of HTGR shutdowns to inspect for degradation, on-line monitoring approaches to manage degradation in HTGRs are needed.

Acoustic emission (AE) and other online monitoring (OLM) technologies, especially guided ultrasonic waves (GUWs), are candidate technologies for performing monitoring and surveillance of HTGR structures while online. The capability of these techniques for monitoring HTGR environments was assessed by performing a survey of open literature relating to operating conditions of HTGRs and the state-of-the-art of AE and GUW techniques. This literature survey consisted of multiple stages including a literature search, a review of abstracts, selecting and requesting literature that was deemed most relevant, and finally a thorough evaluation of the acquired literature. The literature searches were conducted with the assistance of library staff at Hanford Technical Library. Gaps with respect to the application of AE and GUW to HTGR environments are highlighted. Applications of AE to nuclear power plants (NPPs) have been considered for decades and have contributed to the development of leak monitoring, loose parts monitoring, and degradation monitoring systems for LWRs. GUW is an emerging technology for which new applications for NPP monitoring continue to be discovered. Some promising features of GUW techniques with respect to monitoring of HTGR structures are highlighted.

The background noise in HTGRs is a source of uncertainty in predicting the efficacy of AE for the above OLM applications. While cavitation is described as a significant source of noise associated with LWR coolant loops, it will not be a factor in HTGRs. However, oxidation of components at high temperatures may introduce a significant source of noise in HTGRs that is not of consequence to the operation of LWRs. The high temperature of HTGR environments can also negatively impact the effectiveness and reliability of AE monitoring indirectly. Generally, the higher temperature environments in HTGRs relative to LWRs imply a larger standoff requirement for sensitive piezoelectric elements for many reactor components or other heat shielding to limit the thermal exposure of the transducers to tolerable levels. Attenuation in waveguides is linearly related to waveguide length; thus, it is generally expected that AE sensors for HTGR applications will be less sensitive than waveguide sensors for LWR applications.

AE is most sensitive to gross physical damage in materials such as metal loss (corrosion, wear), cracking, and deformation. AE can potentially be deployed for local zone monitoring of degradation processes including corrosion, fatigue cracking, and stress corrosion cracking. In these cases, the monitoring zone may surround an existing flaw or may encompass a region of unusual stress concentration including welds and material discontinuities. The above degradation phenomena are common to both LWRs and HTGRs. Many degradation phenomena unique to HTGRs may be monitored with AE as well. Processes including oxidation, carburization, and creep rupture have all resulted in detectable AE in laboratory experiments employing waveguide sensors. More work may be necessary to fully understand the capability of AE to monitor these processes in HTGR environments and in HTGR-relevant materials.

GUV monitoring is a promising technology with respect to HTGR degradation surveillance. The detection of simulated flaws in LWR components has been demonstrated but difficulties remain with respect to GUV signal interpretation and flaw characterization. GUVs introduced to high-temperature structures will not be subject to attenuation by adjacent layers of liquids, potentially allowing for monitoring during HTGR operation. Additionally, the ability of GUV to monitor structures over a long range may allow for GUV monitoring of structures in harsh conditions remotely from a more tolerable environment.

Acknowledgments

The work described in this report was sponsored by the U.S. Nuclear Regulatory Commission under NRC Job Code Number N6907. Gratitude is reserved for Drs. Amy Hull and Iouri Prokofiev who served as NRC program managers. The effort that Kay Hass expended in the final preparation and formatting of this report is gratefully acknowledged.

Acronyms and Abbreviations

AE	acoustic emission
AET	acoustic emission testing
AGR	advanced gas-cooled reactor
AISI	American Iron and Steel Institute
ARIS	Advanced Reactor Information System
ASME	American Society of Mechanical Engineers
ASNT	American Society of Nondestructive Testing
AST	automatic sensor testing
ASTM	American Society for Testing and Materials
AVR	Arbeitsgemeinschaft Versuchsreaktor
BPV	Boiler and Pressure Vessel
BWR	boiling water reactor
CANDU	CANada Deuterium-Uranium reactor
CFRC	carbon fiber reinforced carbon
Code	ASME Boiler and Pressure Vessel Code
DMDS	dimethyl disulfur
EMAT	electromagnetic acoustic transducers
GTMHR	gas turbine modular helium reactor
GUW	guided ultrasonic wave
HAZ	heat-affected zone
HTGR	high-temperature gas reactor
HTR	high-temperature reactor
HTR-PM	high temperature gas cooled reactor – pebble bed modular
HTTR	high temperature test reactor
IAEA	International Atomic Energy Agency
IGSCC	intergranular stress corrosion cracking
IHX	internal heat exchanger
ISI	inservice inspection
LMFBR	liquid metal (-cooled) fast breeder reactor
LPMS	loose part monitoring systems
LWR	light-water reactor
MARSE	measured area under rectified signal envelope
MHTGR	modular high-temperature gas-cooled reactor
MsS	magnetostrictive sensors
NGNP	next-generation nuclear plant
NPP	nuclear power plant

NRC	U.S. Nuclear Regulatory Commission
ODS	oxide dispersion strengthened
OLM	online monitoring
PBMR	pebble bed modular reactor
PCA	Principle Component Analysis
PCRV	prestressed concrete reactor pressure vessels
PWR	pressurized water reactor
RIS	radiation-induced segregation
RPV	reactor pressure vessel
SCC	stress corrosion cracking
SEM	scanning electron microscopy
SH	shear-horizontal
SiC	Silicon carbide
SOTA	state of the art
SPRT	Sequential Probability Ratio Test
SS	stainless steel
SSC	Systems, structures, and components
TGA	thermogravimetric analysis
TGSCC	transgranular stress corrosion cracking
TLA	thin layer activation
TRISO	tri-structural isotropic (coated-fuel particle design with three materials in coating system (low-density PyC, high-density PyC, and SiC))
UNS	Unified numbering system

Contents

Abstract.....	iii
Summary.....	v
Acknowledgments.....	vii
Acronyms and Abbreviations.....	ix
1.0 Introduction.....	1.1
1.1 Method.....	1.1
1.2 Technical Letter Report Outline.....	1.2
2.0 High Temperature Gas Reactors.....	2.1
2.1 Proposed Structural Materials (Metallic).....	2.3
2.2 Proposed Structural Materials (Non-metallic).....	2.6
2.3 HTGR Environment.....	2.6
2.4 Degradation Mechanisms of Interest in HTGR Maintenance.....	2.7
3.0 Acoustic Emission Monitoring.....	3.1
3.1 Background.....	3.1
3.1.1 Sensitivity of AE to Mechanical Damage (Fatigue and Tensile Failure).....	3.1
3.1.2 Sensitivity of AE to Corrosion and Stress Corrosion Cracking.....	3.2
3.1.3 Sensitivity of AE to High Temperature Mechanisms.....	3.3
3.2 Review of State-of-the-Art in AE/OLM.....	3.5
3.2.1 AE Sensors.....	3.5
3.2.2 Other Hardware.....	3.5
3.2.3 Localization Algorithms.....	3.19
3.2.4 Signal Processing and Analysis.....	3.20
3.2.5 Calibration.....	3.21
3.2.6 Nuclear Power Applications.....	3.22
3.3 Acoustic Emission Codes and Standards.....	3.23
4.0 Guided Wave Monitoring.....	4.1
4.1 Background.....	4.1
4.1.1 Guided Waves in Plates.....	4.1
4.1.2 Guided Waves in Tubes.....	4.3
4.2 GUW Sensors.....	4.4
4.3 Nuclear Power Applications.....	4.7
4.3.1 Containment Liners.....	4.7
4.3.2 Fuel Rod Cladding and Heat Exchanger Tubing.....	4.8
4.3.3 Underground Piping.....	4.9
5.0 AE and HTGR – Discussion.....	5.1
5.1 Applications.....	5.1

5.2	Sensitivity to Relevant Degradation Mechanisms.....	5.1
5.3	Environmental Considerations and Waveguides.....	5.2
5.4	Code Requirements	5.3
5.5	GUW Monitoring.....	5.3
6.0	Summary and Recommendations	6.1
7.0	References	7.1

Figures

2.1	Illustration of a Fuel Kernel, TRISO Fuel Particle, and Spherical Fuel Element of a Pebble Bed Modular Reactor	2.2
3.1	Metal Waveguide AE Sensor Construction	3.6
3.2	Screen Shot Obtained from a Commercial AE System Displaying the Location of AE Events Calculated Using a Multiple Regression Algorithm	3.19
3.3	Example of Data Visualization Capabilities Provided Modern AE Systems Software	3.20
3.4	Photograph of AE Waveguide Attachment and RPV Nozzle at Limerick Unit 1 Reactor	3.23
4.1	Vector Representation of SH Wave Propagation Along the x-direction of a Plate in the Sagittal Plane.....	4.1
4.2	Dispersion Curves Calculated for the Phase Velocity of the First Three SH Modes in an Aluminum Plate	4.2
4.3	Vector Representation of Lamb Wave Propagation Along the x-direction of a Plate in the Sagittal Plane.....	4.2
4.4	Dispersion Curves Calculated for the Phase and Group Velocities of the First Two Antisymmetric and Symmetric Modes in an Aluminum Plate.....	4.3
4.5	Illustration of a) Longitudinal Mode Excitation, b) Flexural Mode Excitation, and c) Torsional Mode Excitation in Tube-Shaped Structures	4.4
4.6	Photograph of an Angle Beam Transducer	4.5
4.7	Drawing of a Comb Transducer	4.5
4.8	Illustration of MsS Guided Wave Injection and Detection Applied to a Steel Pipe	4.6
4.9	Illustration of EMAT Sensor for the Generation of Guided Ultrasonic Waves in a Metal Sample.....	4.7
4.10	Illustration of MsS Applied to Guided Wave Inspection of Fuel Rod Cladding	4.9
4.11	Application of MsS to Guided Wave Inspection of Heat Exchanger Tubing	4.9
4.12	Application of a Comb Transducer to the Inspection of a Pipe	4.10

Tables

2.1	Representative Operational and Conceptual HTGRs.....	2.4
2.2	Summary of Proposed Metallic Materials for HTGR Components.....	2.5
2.3	Summary of Non-metallic Materials for HTGR Components.....	2.6
2.4	Summary of He Impurity Levels Observed During the Operating Experience of Several HTGRs.....	2.6
2.5	Summary of Degradation Mechanisms in HTGRs.....	2.7
3.1	Summary of Studies Investigating the Use of AE for the Detection of Mechanical Damage	3.7
3.2	Summary of Studies Investigating the Use of AE for the Detection of Corrosion and Stress Corrosion Cracking Phenomena.....	3.10
3.3	Summary of Studies Involving the Use of AE to Degradation Phenomena at High Temperatures.....	3.14
3.4	Summary of Several Piezoelectric Materials and Their Properties.....	3.18

1.0 Introduction

Advanced nuclear power plants, such as the Next-Generation Nuclear Plant (NGNP), are expected to operate at higher temperatures to take advantage of the higher efficiencies possible in converting thermal energy to electrical energy. Conventional light-water reactors (LWRs) operate at typical efficiencies of 20%–30% (thermal-to-electric), limited primarily by the coolant. High-temperature gas reactors (HTGRs) are a subset of high-temperature reactors (HTRs) which propose to use a range of coolant materials, including helium or supercritical CO₂ gas, liquid metals (such as liquid sodium), and molten salt to operate at much higher temperatures. HTGR designs are proposed to operate at higher outlet temperatures, on the order of 950°C, which can stress the available materials that are used in the design and construction of the HTGRs. Substantial monitoring and surveillance efforts of structural components are essential to the management of aging and degradation processes in HTGR environments to cope with enhanced material stressors and limited operational experience. In addition, the implementation of on-line refueling (as in the Pebble Bed Modular Reactor) means HTGRs may operate over ten years before encountering a shutdown for fuel management. Ten years is the current inspection interval specified for the inspection of systems, structures, and components (SSCs) in LWRs. Flaw growth rates in HTGRs may be expected to exceed flaw growth rates in LWRs because of higher operating temperatures in HTGRs. To avoid increased frequency of HTGR shutdowns to inspect for degradation, on-line monitoring approaches to manage degradation in HTGRs are needed.

Acoustic emission (AE) and other online monitoring (OLM) technologies, especially guided ultrasonic waves (GUWs), are candidate technologies for performing monitoring and surveillance of HTGR structures while online. The capability of these techniques for monitoring HTGR environments is assessed by reviewing operating conditions of HTGRs and AE state-of-the-art. Gaps with respect to the application of AE to HTGR environments are highlighted. Applications of AE to nuclear power plants (NPPs) have been considered for decades and have contributed to the development of leak monitoring, loose parts monitoring, and degradation monitoring systems for LWRs. GUW is an emerging technology for which new applications for NPP monitoring continue to be discovered. Some promising features of GUW techniques with respect to monitoring of HTGR structures are highlighted.

1.1 Method

Most of the information compiled in this report was obtained from a study of open literature. This literature survey consisted of multiple stages including a literature search, a review of abstracts, selecting and requesting literature that was deemed most relevant, and finally a thorough evaluation of the acquired literature. The focus of the literature search was the physical property studies on the use of acoustic emission, applicability of AE to HTGRs, applicability of GUW to monitoring of NPP SSCs, and existing American Society of Mechanical Engineers (ASME) Boiler and Pressure Vessel Code (Code) provisions related to AE use in nuclear power reactors. Several keywords relevant to AE and GUW, the applicability of AE to HTGRs, applicability of GUW to monitoring of NPP SSCs, and ASME Code sections were identified based on a preliminary literature survey.

These keywords were the basis for a search conducted by Hanford Technical Library to search several databases and identify potentially relevant articles and reports. Searches on these relevant keywords generated a large pool of references related to non-HTGR applications. The pool of generated literature that considered the application of monitoring technologies to HTGRs was relatively sparse. Therefore, a

second phase of the literature search was initiated to identify applications of these technologies in high-temperature plants such as coal and gas-fired plants. In total, the two phases of our literature search identified approximately 900 documents.

Of the approximately 900 documents identified through the literature search, 76 were considered of significant priority to this task. The priority given to individual documents was determined by reviewing document abstracts against several parameters including the age of the document, the application, and uniqueness of the content to reduce the list of documents and minimize document purchases. An additional 40 documents considered of significant priority to this task were identified by reviewing the bibliography obtained in Subtask 1A. Finally, in addition to articles collected through the formal literature search, the authors tracked down articles informally based on an initial evaluation of the literature obtained through the formal literature search.

1.2 Technical Letter Report Outline

This report summarizes the state-of-the-art (SOTA) on AE and other OLM methods (GUW) for monitoring and surveillance of materials in HTGR environments. The remainder of this technical letter report is organized as follows:

- Section 2 summarized aspects of HTGRs considered relevant to the application of AE and other OLM technologies. Likely materials for HTGR components are summarized along with expected degradation mechanisms and representative environmental conditions.
- Section 3 provides a SOTA summary of AE technology. In particular, the sensitivity of AE with respect to several degradation phenomena is summarized. Further, descriptions of modern AE hardware and their capabilities are summarized. Finally, discussions of several applications of AE to the nuclear power industry are included.
- Section 4 discusses GUWs as a monitoring tool for detecting degradation of HTGR SSCs (Systems, Structures, and Components).
- Section 5 highlights gaps and opportunities associated with the application of AE and other OLM technologies to HTGRs.
- Section 6 includes a summary of relevant technical gaps and issues discussed in Section 5.

2.0 High Temperature Gas Reactors

High temperature gas reactors possess several features that distinguish them from LWRs. As their name suggests, HTGRs operate at significantly higher temperatures with outlet coolant temperatures generally greater than 500°C and approaching 950°C. This is accomplished by cooling the reactor using a compressed gas, typically helium. A brief discussion of four significant features of HTGRs (coolant, fuel, reactor pressure vessel, and turbo-machinery) follows.

The Magnox reactors built in the late 1950s in the United Kingdom (UK) represent early gas-cooled reactors. A total of eleven Magnox stations were built in the UK in addition to stations (1 each) in Japan and Italy (Chater 2005). The Magnox reactors were cooled using carbon dioxide and employed graphite moderators. The use of carbon dioxide coolant imposed temperature limitations on the fuel due to fuel-coolant interactions. HTGR designs are able to operate at elevated temperatures due in part to the use of inert helium gas as a coolant (Kupitz and Dee 1984). Helium is also attractive as a coolant for HTGRs because it is not expected to undergo any phase transitions for all conceivable operating and accident scenarios.

In addition to employing helium gas for cooling, operation at higher temperatures in HTGRs is facilitated by the use of coated fuel particles embedded in a graphite matrix. The fuel is composed of small spherical particles of uranium and thorium oxides or carbides 0.2 to 0.6 mm in diameter. Individual particles contain an outer coating of pyrolytic carbon and several inner layers of ceramic material for fission product retention with high-temperature stability (Kupitz and Dee 1984). The particles are homogeneously dispersed in a graphite matrix. The current reference fuel particle design is the tri-structural isotropic (TRISO) particle consisting of four layers of three isotropic materials encasing the fuel kernel (see Figure 2.1). A description of the layers, from innermost to outermost, is provided by Verfondern et al. (2007):

1. A buffer layer of low-density pyrolytic carbon material to accommodate swelling of the fuel kernel, provide void volume for fission gases, and to act as a sacrificial layer for fission products;
2. A coating of high-density pyrolytic carbon to act as a gas-tight coating and diffusion barrier for metallic fission products and to reduce tensile stresses on the SiC (Silicon carbide) layer;
3. A coating of high-density SiC acting as pressure-retaining layer and primary metallic fission product diffusion barrier; and
4. Another coating of high-density pyrolytic carbon to act as a further diffusion barrier for gaseous and metallic fission products, reduce tensile stress on the SiC, protect the SiC during particle handling and sphere/compact formation, and provide a bonding surface for the overcoating.

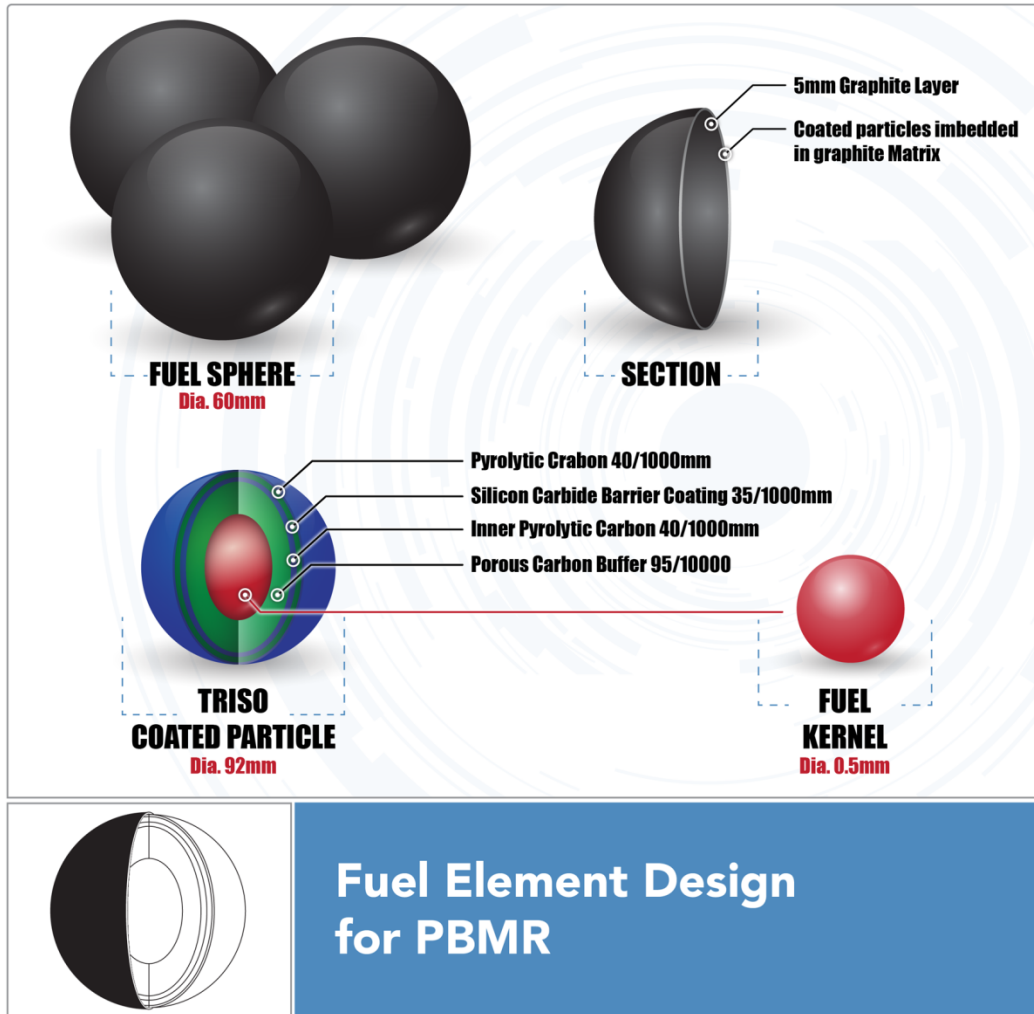


Figure 2.1. Illustration of a Fuel Kernel, TRISO Fuel Particle, and Spherical Fuel Element of a Pebble Bed Modular Reactor

Two primary fuel element designs exist: 1) block or prismatic and 2) spherical. The spherical fuel element design was originally adopted by Germany in the Arbeitsgemeinschaft Versuchsreaktor (AVR) experimental reactor and the THTR-300 prototype reactor. The spherical fuel element was the design selected for the Pebble Bed Modular Reactor (PBMR) sited at Koeberg, South Africa, under consideration by the state-owned utility, Eskom. China has also adopted the spherical fuel element design in the HTR-10 test reactor. Each spherical fuel element has a diameter of 60 mm and contains approximately 12,000 fuel particles embedded in a graphite matrix. No fuel particles are embedded in the outermost 5 mm of the graphite sphere (IAEA 1997). Figure 2.1 is an illustration of the spherical fuel element.

Prismatic or block-type reactors typically consist of large hexagonal blocks of graphite with channels for cooling and insertion of fuel compacts. The fuel compacts consist of fuel particles embedded in a graphite matrix. The fuel compacts can be inserted into the fuel channels of the hexagonal graphite blocks and sealed or they can be integrated into fuel pins, which are inserted into the fuel channels. Each fuel compact contains approximately 10,000 fuel particles (IAEA 1997).

Prestressed concrete reactor pressure vessels (PCRVs) were a common design feature of HTGRs including Fort Saint Vrain, THTR-300, and the advanced gas-cooled reactor (AGR) in the United Kingdom. PCRVs provided several advantages in terms of cost, shielding, functionality, and safety (Beech and May 1999). However, the oil embargo of the 1970s resulted in a dramatic decline in demand for large central electricity generating stations and the accident at Three Mile Island heightened concerns about the safety of nuclear power in the United States. The modular high temperature gas reactor (MHTGR) was designed in response to these developments incorporating a metallic pressure vessel for passive cooling through thermal radiation and preventing the fuel temperature from exceeding 1600°C under accident conditions. Initially designed as 350 MW(t)/135 MW(e) units, the designs were eventually updated to 450 MW(t)/175 MW(e) for economic reasons (La Bar and Simon 1997).

HTGRs have a distinct advantage over LWRs in terms of operating temperature and thermal efficiency. However, it was well recognized that even greater efficiency could be realized by coupling HTGRs directly to a Brayton cycle. Technological barriers prohibited incorporating this feature into HTGRs before the 1990s. A direct Brayton cycle was incorporated into the design of the gas turbine modular high temperature reactor (GT-MHR) with the advent of advances in turbomachinery, recuperators, and magnetic bearing technology. Initiated in the United States by General Atomics, GT-MHR incorporates a prismatic core design. Today, GT-MHR's development continues through an international collaboration. It's currently designed to provide a rated output of 600 MW(t)/287 MW(e) for a conversion efficiency of 48% (La Bar and Simon 1997).

In the United States, only two commercial graphite moderated gas-cooled reactors have been licensed – Fort Saint Vrain and Peach Bottom 1. Plans are underway to develop an HTGR to demonstrate the use of a nuclear heat source for hydrogen production and other industrial applications through the Next Generation Nuclear Plant project (INL 2010b). Still in the conceptualization phase, it is anticipated that NNGP will draw on the experience of PBMR, GT-MHR, and MHTGR concepts.

Three HTGRs are included in the International Atomic Energy Agency's (IAEA) Advanced Reactor Information System (ARIS). These reactors are in various stages of design and conception and include the PBMR, which has received significant investments from South Africa, the Gas Turbine High Temperature Reactor (GTHTR300C), which is the follow-on to Japan's high temperature test reactor (HTTR), and the high temperature gas cooled reactor – pebble bed modular (HTR-PM), which is a follow-on to China's experimental HTR-10. Table 2.1 summarizes characteristics of several worldwide HTGR projects.

In order to discuss on-line monitoring techniques for HTGRs, it is necessary to fully understand the structural materials that HTGRs may be using, the operating environment in which the on-line monitoring techniques may be deployed, and the types of degradation that could occur. Sections 2.1 to 2.4 address each of these topics.

2.1 Proposed Structural Materials (Metallic)

A range of possible materials have been compiled for HTGRs based on previous design experience (Ball and Fisher 2008; INL 2010b). These materials are classified in Table 2.2, accompanied by several attributes and concerns that are mentioned in Murty and Charit (2008). Likely applications of the materials in Table 2.2 were determined based on several documents (Buckthorpe et al. 2001a; Ball and Fisher 2008; INL 2010b) and are included in the final table column.

Table 2.1. Representative Operational and Conceptual HTGRs (Adapted from Kupitz and Dee 1984; Lecomte 1999; Buckthorpe et al. 2001b; Verfondern et al. 2007)

Country	UK	USA	USA	USA	Germany	Germany	South Africa	International	Japan	China
Start/Shutdown	1966/1975	1967/1974	1979/1989	1976/1988	1985/1989					
System	Dragon	Peach Bottom	Fort St. Vrain	AVR	THTR 300	PBMR	GT-MHR	HTTR	HTR 10	
Power, MWt	20	155.5	842	46	750	265	600	30	10	
Core Type	Block	Block	Block	Pebble bed	Pebble bed	Pebble bed	Block	Block	Pebble bed	
He Pressure, MPa	2	2.46	4.8	1	4	7	8	4	3	
Core Inlet, °C	335	343	406	175	262	536	490	395	300	
Core Outlet, °C	835	715	785	580 (950)	750	900	850	850	900	
RPV ID, m	1.07	2.74	5.94	3	5.6	6.2	7.3	5.5	2.5	
Material	Steel	Steel	Concrete	Steel	Concrete	SA508	Mod 9Cr	2¼ CR 1Mo	SA516-70	

Table 2.2. Summary of Proposed Metallic Materials for HTGR Components

Material Class (INL 2010b)	Attributes (Murty and Charit 2008)	Concerns (Murty and Charit 2008)	Applications
Ferritic (T < 450°C) SA 508 SA 533	<ul style="list-style-type: none"> • Extensive experience w/ LWR applications 	<ul style="list-style-type: none"> • Operation at T > 370°C 	<ul style="list-style-type: none"> • Reactor pressure vessel • Cross vessels
Ferritic/Martensitic (T < 650°C) Modified 9Cr-1Mo 2.25Cr-1Mo	<ul style="list-style-type: none"> • Reduced activation property • Void swelling resistance • Creep resistance 	<ul style="list-style-type: none"> • Low long-term creep rupture strength at high temperatures • Irradiation embrittlement at or less than 400°C • Phase stability under neutron irradiation • Radiation-induced segregation 	<ul style="list-style-type: none"> • Reactor pressure vessel
Austenitic stainless steels (T < 800°C) Type 316H stainless steel (SS) Type 304 SS Type 347 SS	<ul style="list-style-type: none"> • Creep resistance at higher temperatures • Reasonable corrosion/oxidation resistance 	<ul style="list-style-type: none"> • Phase stability under neutron irradiation • Radiation-induced segregation • Radiation-assisted intergranular stress corrosion cracking (IGSCC) • Irradiation creep • Void swelling • Thermal creep • Corrosion resistance at high temperatures 	<ul style="list-style-type: none"> • Internal core structural components • Ducting • Recuperators
Ni-based Alloys (T < 1050°C) Inconel 617 Incoloy 800H Hastelloy X/XR Haynes 230 Inconel 740	<ul style="list-style-type: none"> • Creep properties • High temperature strength 	<ul style="list-style-type: none"> • Radiation embrittlement • Irradiation swelling • Phase stability under neutron irradiation • High temperature He embrittlement could be an issue 	<ul style="list-style-type: none"> • Internal core structural components • Intermediate Heat Exchangers • Control Rods • Turbomachinery
Oxide Dispersion Strengthened (ODS) steels (T < 1100°C)	<ul style="list-style-type: none"> • High-temperature properties • Resistance to radiation swelling • Resistance to radiation embrittlement 		<ul style="list-style-type: none"> • Internal core structural components
Refractory metals (T < 1400°C)	<ul style="list-style-type: none"> • Creep resistance to high burn-ups • Swelling resistance to high burn-ups 	<ul style="list-style-type: none"> • Oxidation resistance • Low temperature radiation embrittlement • Joining 	<ul style="list-style-type: none"> • Internal core structural components

2.2 Proposed Structural Materials (Non-metallic)

Non-metallic materials have also been proposed for certain structural components of HTGRs—particularly internal components exposed to high temperatures. Relevant non-metallic materials include nuclear grade graphite, ceramics, and composite materials. Table 2.3 summarizes candidate non-metallic materials and their possible HTGR applications based on information contained in NUREG/CR-6944 (Ball and Fisher 2008), INL/EXT-09-17187 (INL 2010b), and Buckthorpe et al. (2001a).

Table 2.3. Summary of Non-metallic Materials for HTGR Components

Non-metallic Materials		Application
Graphite		Internal core structural components
Ceramics	<ul style="list-style-type: none"> • Baked carbon • Quartz • Alumina • Silica • Kaowool 	Internal core structural components
Composites	<ul style="list-style-type: none"> • C-C • SiC-SiC • Carbon fiber reinforced carbon (CFRC) 	Control rods

2.3 HTGR Environment

Typical HTGRs will have outlet coolant temperatures approaching 950°C with the pressure boundary temperature maintained at less than 370°C for “cold” vessels and approaching 500°C for “warm” vessels (Table 2.1). Coolant is most likely provided by helium flow at pressures approaching 10 MPa (Table 2.1). A summary of He impurity levels observed during the operation of several HTGRs is provided in Table 2.4 (Ball and Fisher 2008; INL 2010b).

End of life neutron fluences for HTGR reactor pressure vessels (RPVs) are at least an order of magnitude less than for LWR RPVs (INL 2010b), which have end of life fluences of greater than 10^{17} n/cm² (BWRs) (IAEA-TECDOC-1470, IAEA 2005) and 10^{18} n/cm² (PWRs) (IAEA-TECDOC-1556, IAEA 2007). Neutron fluence levels for the core support structures and other metallic internals are typically below 1×10^{19} n/cm². Components in close proximity to the pebble fuel are subjected to the highest fluence levels of slightly above 1.1×10^{22} n/cm² (INL 2010b).

Table 2.4. Summary of He Impurity Levels (μbar) Observed During the Operating Experience of Several HTGRs (INL 2010a)

HTGR	H ₂ O	H ₂	CO	CO ₂	CH ₄	O ₂	N ₂
Dragon	0.1	0.1	0.005	0.02	0.1	0.1	0.05
Peach Bottom	0.5	10	0.5	<0.05	1.0	-	0.5
Fort St. Vrain	1	7	3	1	0.1	-	-
AVR	0.15	9	45	0.25	1		22
THTR	<0.01	0.8	0.4	0.2	0.1		0.1

2.4 Degradation Mechanisms of Interest in HTGR Maintenance

HTGRs are susceptible to familiar forms of degradation including fatigue, stress-corrosion cracking, and corrosion, as well as new forms of degradation introduced by the high temperatures and gas coolant.

RPV materials will be exposed to modest neutron fluences and temperatures relative to the reactor internal components. The main degradation concerns associated with RPVs include fatigue, fracture, and creep-fatigue (Buckthorpe et al. 2001a).

High-temperature components include RPV internal components, intermediate heat exchangers, and turbomachinery. Austenitic stainless steels, nickel alloys, graphite, ceramics, and composites are all materials considered for internal components. Austenitic stainless steels are susceptible to radiation affects including void swelling, radiation-induced segregation, phase instability, radiation-assisted IGSCC, and irradiation creep. Austenitic steels may also be vulnerable to thermal creep and corrosion due to exposure to He impurities at high temperature. Nickel alloys may be vulnerable to radiation affects including void swelling and radiation embrittlement. They may also be susceptible to He embrittlement at high temperature.

For graphite exposed to He impurities at high temperature, oxidation is a significant concern (Buckthorpe et al. 2001a) in addition to swelling or shrinkage caused by neutron irradiation (INL 2010b). He impurities introduce other damage mechanisms including corrosion, erosion-corrosion, carburization, and decarburization. For turbomachinery, creep-related dimensional changes in blades can lead to catastrophic failure (Buckthorpe et al. 2001a). Table 2.5 is a summary of HTGR degradation mechanisms.

Table 2.5. Summary of Degradation Mechanisms in HTGRs

Creep Effects	<ul style="list-style-type: none"> • Creep-rupture • Creep-fatigue • Creep-buckling
Helium Impurity Effects	<ul style="list-style-type: none"> • Corrosion • Erosion-corrosion • Oxidation • Carburization • Decarburization
Thermal Aging	<ul style="list-style-type: none"> • Reduction in yield and ultimate tensile strength • Cyclic softening
Thermal Fatigue	<ul style="list-style-type: none"> • Cracking
Irradiation Effects	<ul style="list-style-type: none"> • Irradiation embrittlement • Irradiation swelling • Radiation-induced phase transitions (Murty and Charit 2008) • Radiation-induced segregation (RIS) (Murty and Charit 2008) • Radiation-assisted IGSCC • Irradiation creep

Special concern is associated with weldments and other structural discontinuities that can lead to stress concentration (O'Donnell et al. 2008) and with intermediate heat exchangers. Internal heat exchangers (IHXs) consist of thin-walled tubes (possibly nickel alloy) exposed to high-temperature He and large pressure differentials. The Phenomena Identification and Ranking Table (PIRT) technique was used to identify safety-relevant/safety-significant phenomena and assess the importance and related knowledge base of high-temperature structural materials issues for NGNP. Through this process, several issues were identified as having special significance as the phenomena were considered high priority issues for which limited knowledge exists (Corwin et al. 2008, NUREG/CR-6944, Vol. 4). These issues can be summarized as follows:

- Thermal aging and crack initiation and growth in 9Cr-1Mo steel are a concern particularly due to the lack of practical knowledge/experience regarding the behavior of 9Cr-1Mo.
- Compromise of emissivity for the RPV and RPV internals is of concern as maintaining high emissivity is important for passive cooling. Only a few studies on stainless steel and SA508 steel exist for which to base expectations regarding maintaining high emissivity.
- IHX failure is a concern due to creep effects and the difficulties expected in inspecting compact heat exchangers.
- Radiation creep of RPV internals is a concern especially with respect to effects in Alloy 800H. Little information is available to assess irradiation creep effects in Alloy 800H and dimensional changes as a result of Alloy 800H are a concern.
- Generic failure of non-metallic components in HTGR-relevant environments is a concern due to a lack of experience. There is a need to assess microstructural stability and thermophysical properties during irradiation and high-temperature exposure to He.
- The capability of large valves to maintain He leak tightness is a concern due to limited knowledge (despite past operating experience) and He tribology effects. In addition, studies are needed to assess acceptable levels of He leakage in valves.

3.0 Acoustic Emission Monitoring

3.1 Background

A detailed history and introduction to acoustic emission testing is provided in the American Society of Nondestructive Testing (ASNT) Handbook (ASNT 2005). Fundamentally, acoustic emission is the elastic energy released during deformation of materials (ASNT 2005). The released energy travels as a transient elastic wave in the material and is typically recorded using a transducer that is located at some distance from the AE source. In metals, several phenomena give rise to AE, including crack initiation and growth, phase transformations, twinning, deformation, etc. Factors such as leaks also give rise to changes in the local stress gradients, resulting in a transient elastic wave.

3.1.1 Sensitivity of AE to Mechanical Damage (Fatigue and Tensile Failure)

For metals experiencing mechanical degradation, several phenomena can be responsible for the generation of AE. These phenomena include:

- Dislocation generation and motion (Mukhopadhyay et al. 1998; Mukhopadhyay et al. 2000; Pollock 2003; Shaira et al. 2008)
- Martensite formation (Dukes and Culpan 1984; Mukhopadhyay et al. 1998; Mukhopadhyay et al. 2000; Shaira et al. 2008)
- Twinning (Dukes and Culpan 1984; Pollock 2003; Shaira et al. 2008)
- Fracture and decohesion of inclusions and precipitates (Dukes and Culpan 1984; Pollock 2003; Shaira et al. 2008)
- Plastic deformation (Sinclair et al. 1977; Moorthy et al. 1994; Pollock 2003; Rogers 2005)
- Crack propagation (Harris and Dunegan 1974; Berkovits and Fang 1995; Pollock 2003; Rogers 2005; Shaira et al. 2008)
- Crack closure/rubbing (Harris and Dunegan 1974; Sinclair et al. 1977; Moorthy et al. 1994; Berkovits and Fang 1995).

Several of the above phenomena exhibit distinct behaviors with respect to time. AE from crack propagation and decohesion of inclusions and precipitates are discontinuous and occur as discrete “bursts” of energy (Harris and Dunegan 1974), while dislocation motion and generation processes result in the continuous release of energy (Mukhopadhyay et al. 1998; Mukhopadhyay et al. 2000). Commercial grade 304 stainless steel is shown to generate more AE activity than nuclear grade 304 stainless steel, and this is attributed to the increased concentration of precipitates and inclusions in the commercial grade steel. In these studies, AE caused by fracture and decohesion of inclusions and precipitates served as the dominant AE source mechanism in the commercial grade steel compared to the nuclear grade steel in which dislocation motion and generation was the dominant source mechanism. Further, it is concluded that the presence of strain localizations such as notches and cracks could cause martensite transformations to act as the dominant AE source mechanism (Mukhopadhyay et al. 1998; Mukhopadhyay et al. 2000). Table 3.1 is a summary of several studies related to monitoring mechanical damage phenomena in several metals.

Measurements of crack growth are most frequently obtained in the linear fracture mechanics regime. In this crack growth regime, crack growth rate (da/dt) is related to the stress-intensity factor ($\Delta K = K_{\max} - K_{\min}$) by Paris's Law where $K_{\max}(K_{\min})$ is the maximum(minimum) stress intensity experienced at the crack tip:

$$da/dcycles = C * (\Delta K)^n \quad (3.1)$$

C and n are empirically derived constants. AE activity may also be related to ΔK by a similar relation, where N represents a cumulative AE metric and A and m are empirically derived constants:

$$dN/dcycles = A * (\Delta K)^m \quad (3.2)$$

In Eq. (3.2), N could represent any of several AE activity metrics including the number of AE counts, hits, events, and amount of energy release. In practice, the relationships (3.1) and (3.2) above are combined so that crack growth rate may be inferred from AE activity,

$$da/dt = \left(C / (A^{n-m}) \right) (dN / dt)^{n-m} \quad (3.3)$$

Section V, Article 13 of the ASME Code specifies $n - m = 0.53$ and $(C / (A^{n-m})) = 290$ where N refers to the number of events and da/dt has units of microinches/second.

The relationship in Eq. (3.2) has generally been validated for various materials under plane strain fracture conditions (Sinclair et al. 1977; Chen and Choi 2004). However, several studies have shown that AE behavior is significantly impacted as the fracture mode transitions from plane strain to plane stress conditions. For austenitic stainless steels, crossing over from plane strain to plane stress conditions results in a dramatic decrease in AE activity (Yuyama et al. 1984; Moorthy et al. 1994).

Crack propagation is physically characterized as a series of discrete jumps of length Δl . The length of the crack jump is determined by the size of the plastic zone at the crack tip that undergoes work hardening until the local stress intensity factor exceeds a threshold value, ΔK_{th} . It's reported that 100 μm represents a typical value for Δl (Rogers 2005). During fatigue testing of flat Incoloy 901 test specimens minimum detectable crack lengths between 50–100 μm were observed (Berkovits and Fang 1995). In addition, Harris and Dunegan (1974) reported a threshold crack growth rate of 2.5×10^{-8} m/cycle for AE monitoring of fatigue crack growth in 7075-T6 aluminum and 4140 steel. Table 3.1 is a summary of studies investigating the use of AE to study mechanical damage in several metals.

3.1.2 Sensitivity of AE to Corrosion and Stress Corrosion Cracking

Generally, the mechanisms responsible for AE during corrosion are not characterized as well as mechanisms responsible for AE from mechanical damage (Lenain and Proust 2005). Some of the corrosion processes that could result in AE are (Shaikh et al. 2007).

- Film cracking
- Gas evolution
- Hydrogen migration

- Plastic zone formation
- Stress corrosion cracking (SCC)
- Hydrogen cracking

The evolution of gas by cathodic reactions and the breakdown of thick surface oxide films have also been identified as suspected sources of AE during SCC and corrosion processes by Yuyama et al. (1984). In addition, it is noted that several phenomena can contribute to total detectable AE during crack extension, including the following (Yuyama et al. 1984):

- Martensitic transformation
- Slip deformation
- Twinning
- Fracture and decohesion of precipitates, second-phase particles, or non-metallic inclusions
- Microcracking

Corrosion processes accompanying SCC can mask the AE signals produced by cracking (Yuyama et al. 1984; Jones and Freisel 1992) unless signals produced by corrosion processes can be distinguished from SCC. Discrimination between AE activity from corrosion processes and cracking is often based on amplitude as cracking signals are more energetic than signals released by corrosion processes (Ramadan et al. 2008). It has been observed in the laboratory that transgranular stress corrosion cracking (TGSCC) and IGSCC processes can result in different levels of AE activity. AE monitoring of SCC in American Iron and Steel Institute (AISI) 304 stainless steel has shown that TGSCC is an order of magnitude more active than IGSCC in terms of AE (Alvarez et al. 2008). Table 3.2 is a summary of several studies related to monitoring corrosion and SCC damage phenomena in several metals.

AE monitoring was used to investigate IGSCC growth in Inconel 600. The reported minimum detectable crack size from AE monitoring is 200 to 400 μm in length and 100 μm in depth (Sung et al. 1997). This agrees well with the result of IGSCC crack initiation studies in 304 stainless steel. In these studies, the minimum detectable crack dimensions are reported as 200–300 μm in length and 100–200 μm in depth (Jones et al. 1991). Minimum detectable crack growth rates of 10^{-7} m/s for IGSCC in Inconel 600 steel (Sung et al. 1997) and 2.33×10^{-8} m/s for TGSCC in 316 stainless steel have been reported (Shaira et al. 2008). Further, it is indicated that IGSCC of 304 stainless steel has a specific AE activity of approximately 20 events/ mm^2 (Jones and Freisel 1992). Crack growth rate is related to AE activity through relationship (3.3). However, for SCC, the empirical constants are dependent on environmental parameters.

3.1.3 Sensitivity of AE to High Temperature Mechanisms

AE monitoring has been applied to study several high temperature damage related phenomena including creep rupture (Clark et al. 1982), metal dusting (Ferrer et al. 2001), oxidation (Walter et al. 1993), and coke deposition (Ropital et al. 2004). Creep rupture on the heat-affected-zones (HAZs) of CrMoV steel welds were monitored with AE to temperatures of 690°C. PZT 5A sensors with a Curie temperature of 350°C were mounted on the end of waveguides to perform the high temperature monitoring. A commercial coating referred to as “Berkatekt 29” was applied to the surface of the test

specimen to prevent oxidation and subsequent noise caused by cracking and spalling of oxide film. The microstructure was observed to have a significant impact on the generation of AE. Cracks propagate rapidly through coarse microstructures with the majority of AE activity occurring just before failure. Crack growth is repeatedly arrested in fine grain microstructures resulting in step-wise crack growth and corresponding “bursts” of AE (Clark et al. 1982).

AE monitoring has also been employed at high temperatures to study metal dusting (catastrophic carburization) of UNS N08810 (alloy 800H) at temperatures up to 650°C. Metal dusting is described as an important damage phenomenon in thermal cracking and ammonia process plants. In particular, AE testing was employed to assess the effectiveness of dimethyl disulfur (DMDS) for inhibiting the metal dusting phenomenon. It is noted that metal dusting develops uniformly in carbon steels and low alloy steels, but for stainless steels and nickel based alloys, it grows by pitting. Metal dusting is characterized by an incubation period during which it remains acoustically inactive. After metal dusting is activated, AE activity exhibited linear behavior. Tests were conducted on a pipe specimen with wide-band AE transducers mounted on each end through waveguides. Coke deposition on the wall of the pipe caused AE activity to cease. It is speculated that AE activity associated with coke deposition was below the system threshold (Ferrer et al. 2001).

AE has been used in combination with thermogravimetric analysis to study the effectiveness of hydrogen sulfide as an inhibitor of coke deposition on Ni, α -Fe, γ -Fe, Co, V, Mo, and Cr metals. It is noted that the formation of carbon filaments in the range of temperatures 450°C–700°C is a major problem in many chemical and petrochemical processes where hydrocarbons or other carburizing atmospheres are involved. In carburizing and reducing atmospheres, reactions induce fragmentation of the oxide scale and the formation of graphite on the iron surface. AE results showed good correlation to thermogravimetric analysis and injection of hydrogen sulfide, indicating that AE is sensitive to coke deposition. In these studies, a 300-kHz resonant transducer is coupled to the test specimen through a quartz filament, which acts as a waveguide (Ropital et al. 2004).

Oxide films serve as a protective layer of metals exposed to high temperature environments and AE has been deployed in several studies aimed to observe the degradation of these protective oxide layers. AE from oxide layers is caused by stress that can build-up due to 1) the effects of mismatched thermal expansion coefficients between metal and film upon temperature cycling and 2) isothermal growth stresses (Schmutzler and Grabke 1993). Cracking and spalling of oxide films were observed with AE upon thermal cycling of alloy 800H from 900°C to 100°C and thermal cycling of HK 40 steel from 950°C to 200°C (Walter et al. 1993). Generally, more stress accumulates from thermal cycling than isothermal growth, resulting in much greater AE activity. Studies of the oxidation behavior of high Al and Cr alloys were implemented using AE and thermo-gravimetric analysis. Specimens underwent thermal cycling from 1000°C to room temperature. In these tests, detectable AE was observed during isothermal growth conditions (Schmutzler and Grabke 1993). Further studies were conducted on 20Cr-25Ni-Nb stainless steel to observe the oxide film integrity under thermal cycling and isothermal growth conditions at temperatures up to 1000°C. In these studies, no AE was observed during isothermal growth conditions and it was established that oxide cracking preceded spalling (Bennett et al. 1989). In all of these studies, sensors are coupled to test specimens through waveguides. Table 3.3 is a summary of several studies related to monitoring high temperature damage phenomena in several metals.

3.2 Review of State-of-the-Art in AE/OLM

3.2.1 AE Sensors

Sensors for AE monitoring are based on piezoelectric materials. The most relevant piezoelectric parameters include the Curie temperature, T_c which limits the highest operating temperature of the sensor, and the coupling factor, k_{33} , which determines the sensitivity. An overview of piezoelectric materials is provided by Griffin et al. (2009) including a table of piezoelectric materials and several of their properties. This table is also provided here as Table 3.4 for convenience. It is important to note the trade-off that exists between T_{max} and k_{33} . For PZT-5A, $T_{max} = 365^\circ\text{C}$ and $k_{33} = 70\%$ while, for lithium niobate, $T_{max} = 1000^\circ\text{C}$ and $k_{33} = 15\%$. A review of high temperature transducers available from one vendor indicates that they are limited to applications for $T < 540^\circ\text{C}$ (PAC 2005). The literature indicates that the life-limiting neutron fluence for lead zirconate titanate transducers is near 10^{15} n/cm². Data is unavailable to assess the life limiting neutron fluence of lithium niobate (Griffin et al. 2009). Recent testing of aluminum nitride has shown that this piezoelectric material is hardened to the following radiation levels: fast neutron fluence of 1.85×10^{18} n/cm², thermal neutron fluence of 5.8×10^{18} n/cm², and a gamma radiation dose of 26.8 MGy (Parks and Tittmann 2011).

Metallic waveguides can be used to isolate sensitive AE transducer components from harsh temperature or radiation environments. Two field demonstrations of the use of AE to detect flaw growth in nuclear reactor pressure vessel components were implemented using waveguides (see Figure 3.1) (Hutton et al. 1984; Hutton et al. 1993). Attenuation in 3.2-mm (1/8-in.) diameter rod-shaped stainless steel waveguides is reported to be 1.5 dB/m (Hutton 1993). Rules for using waveguides for harsh environment monitoring are included in mandatory Appendix V of Article 13, Section V of the ASME Boiler and Pressure Vessel Code (ASME 2010). The recommendation is provided to limit waveguide length to 6 m. The interfaces between the waveguide and test component and the sensor and waveguide result in additional signal attenuation. For pressure coupled waveguides, best acoustic coupling is observed above 110 MPa of coupling pressure (ASME 2010).

3.2.2 Other Hardware

The output of an AE sensor is routed through a pre-amplifier on its way to the main signal processor. At the preamplifier, a bandpass filter is applied to the signal along with gain (20 dB, 40 dB, and 60 dB are typical gain options). Preamplifier noise and dynamic range are significant parameters with respect to preamplifier functionality. A survey of specifications for preamplifiers available from one commercial supplier indicates that noise levels less than $10 \mu\text{V}_{\text{rms}}$ and dynamic ranges near 80 dB are typical (PAC 2005). The electronic noise level introduced by preamplifiers is limited to less than $7 \mu\text{V}_{\text{rms}}$ for nuclear components per Appendix I of Articles 13, Section V of the ASME Code.

Other AE system components include signal cables, the signal processor, and the display monitor. Functionally relevant parameters associated with signal cables include electromagnetic shielding and attenuation specifications. Article 13, Section V of the ASME Code specifies the use of coaxial cables.

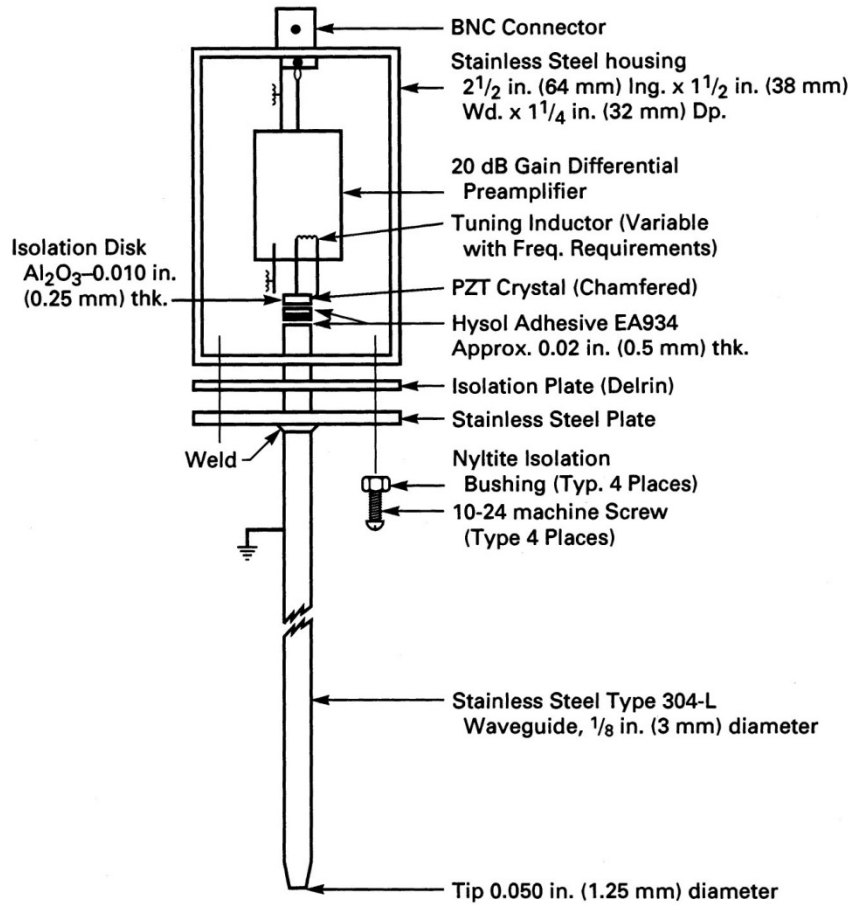


Figure 3.1. Metal Waveguide AE Sensor Construction (ASME 2010). Reprinted from ASME 2010 BPVC, Section V, by permission of The American Society of Mechanical Engineers. All rights reserved.

Table 3.1. Summary of Studies Investigating the Use of AE for the Detection of Mechanical Damage

Reference/Purpose	Material	Notes/Results
(Mukhopadhyay et al. 1998; Mukhopadhyay et al. 2000)	Commercial and nuclear grade 304 SS	<ul style="list-style-type: none"> Dislocation generation and motion is the dominant source of AE in nuclear grade 304 SS whereas fracture and decohesion of inclusions dominates in commercial grade 304 SS Overall, magnitude of AE activity greater in commercial grade 304 SS versus nuclear grade 304 SS Dislocation generation and motion results in continuous AE activity while fracture and decohesion of inclusions results in more burst-like activity
Study of AE activity vs. ΔK relationship for notched and un-notched specimens		<ul style="list-style-type: none"> In notched specimens, strain localization at crack tip expected to lead to significantly more AE due to martensite formation vs. dislocation generation and motion
(Dunegan et al. 1970)	7075-T6 aluminum and 4140 steel	<ul style="list-style-type: none"> Is noted that crack closure is a source of AE that can interfere with crack growth measurements Indicated that the rise time of AE signals from crack closure or fixture noise is slower relative to AE signals from crack growth The “burst” type of behavior from crack growth is noted with the count rate high for a few cycles of loading followed by a period of inactivity Threshold crack growth rate for AE activity estimated as 2×10^{-8} m/cycle Load cycling rate does not affect the observed acoustic emission activity
(Chen and Choi 2004)	2014-T6 aluminum, 7050-T76511 aluminum, and ASTM* A36 steel	<ul style="list-style-type: none"> For aluminum specimens, signals cluster between 35 and 55 dB and up to 2000 μs in duration; for steel specimens – 30–50 dB up to 2500 μs... some signals beyond 65 dB Observed linear relationship between AE parameters (cumulative hits, hit rate, cumulative AE energy) vs. max stress intensity factor Observed drastic increase in AE activity correlating with sharp increase with max stress intensity factor after a certain number of cycles indicating the presence of two crack-growth regimes Attribute softness or ductile nature of the steel sample to the reduction in observed AE activity
(Sinclair et al. 1977)	A533 steel, H1 weld metal, low carbon steel	<ul style="list-style-type: none"> Study AE associated with fatigue crack growth in three specimens (A533 steel, low carbon steel pipe, H1 weld metal) Observed increase with AE activity with increase in ΔK Increasing ΔK resulted in a change in the amplitude distribution of AE data (for A533 steel) Is suggested that AE is associated with crack “opening/closing” mechanism and microfracture immediately ahead of the crack tip
Study AE associated with fatigue crack growth in three specimens		

Table 3.1. (cont'd)

Reference/Purpose	Material	Notes/Results
(Moorthy et al. 1994)	AISI 316	<ul style="list-style-type: none"> • Noted that two sub-regimes (stage IIa and IIb) are observed in stage II • The transition from stage IIa to IIb has been accompanied by a sharp increase in crack propagation rate and sharp decrease in AE activity • Suggested that stage IIa is microstructure sensitive and constitutes slow growth, while IIb is insensitive to microstructure and characterized by rapid growth • Plots of AE activity versus ΔK show a peak at the transition from IIa to IIb • Of the AE sources considered; crack growth, crack opening/closing, and plastic deformation - plastic deformation at the crack tip is considered the dominant source.
(Berkovits and Fang 1995)	Incoloy 901	<ul style="list-style-type: none"> • Reported that crack initiation evident in histograms of events vs. stress and cycle as events occur near zero stress due to crack opening/closure • Crack initiation was determined by AE peak onset...revealed initial crack lengths of between 50–100 μm • Plastic flow during tensile part of cycle results in compressive residual stress that causes crack rubbing at non-zero stress levels.
AE monitoring of fatigue degradation of Incoloy 901 flat test specimen		<ul style="list-style-type: none"> • AE histogram indicates that crack rubbing ceases before maximum compressive load is reached • Crack closure of a small crack occurs at a lower stress than a long fatigue crack • Crack closure stress for a long fatigue crack is independent of the crack length • AE count rate shows linear relationship with stress intensity factor except near the threshold • AE emissions associated with crack growth are stress and life-time dependent

Table 3.1. (cont'd)

Reference/Purpose	Material	Notes/Results
(Shaira et al. 2008)	304L stainless steel	<ul style="list-style-type: none"> The following mechanisms of AE have been confirmed in AISI 304L stainless steel <ul style="list-style-type: none"> Dislocation motion Formation of martensite Twin formation Inclusion fracture Crack nucleation Crack propagation
AE monitoring of fatigue tests on 304L specimens and use of k-means data clustering method for signal processing		<ul style="list-style-type: none"> AE signals collected from tests performed in actual conditions must be segmented into clusters based on closest similarities Martensitic transformation can appear under cyclic loading at room temperature Dislocation avalanche should correspond to fairly long events Twinning should result in high-amplitude AE bursts Microcracks expected to produce AE over a range of energies
(Rogers 2005)	BS 4360 grade 50C structural steel	<ul style="list-style-type: none"> Crack propagation is not continuous but occurs in discrete, high-velocity steps Minimum detectable crack size 100 μm–200 μm
Performed fatigue study of BS 4360 grade 50C structural steel		<ul style="list-style-type: none"> Experience has shown that interference from laboratory fatigue machinery is typically more severe than the application environment Performed fatigue study of BS 4360 grade 50C structural steel – discovered three bands of AE signals associated with plastic deformation, instrumentation noise, and macro crack propagation.

*ASTM = American Society for Testing and Materials

Table 3.2. Summary of Studies Investigating the Use of AE for the Detection of Corrosion and Stress Corrosion Cracking Phenomena

Reference/Purpose	Material	Notes/Results
(Zhang et al. 2008) AE monitoring of commercial 304H stainless steel at constant loads of 180 or 90 MPa – results correlated with electrochemical measurements	304H stainless steel	<ul style="list-style-type: none"> • Results indicate that AE is only sensitive to rapid cracking propagation but not SCC initiation and early stage propagation. It is postulated that AE is sensitive to SCC mechanisms resulting in large areas of plastic deformation but insensitive by SCC events accompanied by small scale or minor plastic deformation. • Proposed mechanism for SCC initiation and propagation includes slow anodic dissolution at chromium depleted grain boundaries. Then, sulfur adsorption on the surface around the crack tip catalyzes the entry of hydrogen atoms generated by hydrogen reduction reactions into the steel ahead of the crack tip where it gradually accumulates and eventually leads to hydrogen induced cracking along grain boundaries.
(Sung et al. 1997) AE monitoring of SCC in Inconel 600 alloy for several different heat treatments and constant strain rates	Inconel 600 alloy	<ul style="list-style-type: none"> • Plastic deformation produced signals of lower amplitude than IGSCC and ductile fracture. • Widest AE amplitude distributions associated with discontinuous crack growth process in brittle high-strength metal while the growth of the plastic zone prior to crack extension gives relatively narrow amplitude distributions • Observe a linear relationship between SCC susceptibility and width of amplitude distributions • 3 phases of SCC crack growth identified: 1) generation of small cracks at the surface, 2) growth of small cracks and formation of dominant cracks, 3) growth of dominant cracks and fracture • Minimum crack size detectable with AE is 200 to 400 μm in length and below 100 μm in depth

Table 3.2. (cont'd)

Reference/Purpose	Material	Notes/Results
(Shaikh et al. 2007)	AISI 316LN	<ul style="list-style-type: none"> Noted that AE can be caused by atomistic damage such as dislocation motion or due to macroscopic processes such as deformation, corrosion, and growth
AE monitoring of SCC in AISI 316LN stainless steel to determine the mechanism of SCC at 413K and in a 45% MgCl ₂ solution at constant load		<ul style="list-style-type: none"> Dissolution of metal or film should not produce AE because neither results in a strain on the lattice Is noted that the following corrosion processes could lead to AE generation (because they strain lattice) <ul style="list-style-type: none"> ◆ Film cracking ◆ Gas evolution ◆ Hydrogen migration ◆ Plastic zone formation ◆ Discontinuous cracking during SCC ◆ Hydrogen cracking Is stated that each process has a definite range of amplitudes and frequencies that should make each signal distinguishable Crack growth rate of 2.33×10^{-8} m/s observed in the plateau region Suggested that AE signals between 27.6–39.8 dB are due to dislocation motions during plastic deformations Signals from plastic deformation in pre-crack tip area had amplitudes from: 31–34 dB and rise times of less than 120 μs AE signals with amplitudes of 40.9–46.5 dB and rise times greater than 120 μs are likely due to hydrogen evolution AE signals with amplitudes of 40.9–46.5 dB and rise times less than 120 μs are likely due to plastic deformation Its observed that the rate of AE parameters decreased with increasing crack growth rate AE was rather continuous and included the signals with highest observed amplitudes prior to initiation In the initiation, slow propagation stage, and fast propagation stages, time between AE's increased and the energy per emission tended to decrease slightly Indicated that majority of AE caused by plastic deformation at crack tip Cracking found to initiate and propagate in transgranular mode

Table 3.2. (cont'd)

Reference/Purpose	Material	Notes/Results
(Alvarez et al. 2008)	AISI 304 SS	<ul style="list-style-type: none"> Plastic deformation studies in air revealed most AE signals to occur near the yield point of the load curve and decreases thereafter until final failure Mean event rate during TGSCC found to be an order of magnitude higher than during testing in air Mean event rate during IGSCC found to be a little higher than during testing in air Mean amplitude and mean rise times of TGSCC and IGSCC signals found to be similar – these amplitudes are smaller than those from plastic deformation and have longer rise times Classification of source mechanisms reveals that TGSCC and IGSCC signals originate from the same source mechanism Postulated that the source of AE signals for TGSCC and IGSCC is the mechanical tearing of the metallic ligaments left behind by the propagating crack
AE monitoring of SCC of solubilised and sensitized type AISI 304 stainless steel at constant strain rates in solution of 1 M NaCl + 1 M HCl	Eutectoid cold drawn steel	<ul style="list-style-type: none"> Localized corrosion and stress corrosion cracking are the most frequent forms of corrosion, particularly in a marine environment Observed AE signals clustered into 3 groups: initiation, crack propagation, and failure Crack propagation rate of 10^{-7} m/s Crevice and pitting corrosion observed during the test All AE activity occurred during 14 hr span - No AE activity observed during first 900 hrs of experiment. The amplitude of collected events used as parameter to distinguish between SCC and other corrosion processes Energy relaxation events because of SCC are considered much larger than energy release events during localized corrosion Principle Component Analysis (PCA) and K-mean clustering are used to classify signals Scanning electron microscopy (SEM) analysis revealed crack propagation by transgranular mode The crack initially propagates in mode I (shear cracking-like mechanism) and transitions to mode II (cleavage-like mechanism) after a certain subcritical growth
(Ramadan et al. 2008)	Eutectoid cold drawn steel	<ul style="list-style-type: none"> Localized corrosion and stress corrosion cracking are the most frequent forms of corrosion, particularly in a marine environment Observed AE signals clustered into 3 groups: initiation, crack propagation, and failure Crack propagation rate of 10^{-7} m/s Crevice and pitting corrosion observed during the test All AE activity occurred during 14 hr span - No AE activity observed during first 900 hrs of experiment. The amplitude of collected events used as parameter to distinguish between SCC and other corrosion processes Energy relaxation events because of SCC are considered much larger than energy release events during localized corrosion Principle Component Analysis (PCA) and K-mean clustering are used to classify signals Scanning electron microscopy (SEM) analysis revealed crack propagation by transgranular mode The crack initially propagates in mode I (shear cracking-like mechanism) and transitions to mode II (cleavage-like mechanism) after a certain subcritical growth
AE monitoring of SCC in cables (eutectoid cold drawn steel – 7 strand wires) of prestressed concrete structures	Eutectoid cold drawn steel	<ul style="list-style-type: none"> Localized corrosion and stress corrosion cracking are the most frequent forms of corrosion, particularly in a marine environment Observed AE signals clustered into 3 groups: initiation, crack propagation, and failure Crack propagation rate of 10^{-7} m/s Crevice and pitting corrosion observed during the test All AE activity occurred during 14 hr span - No AE activity observed during first 900 hrs of experiment. The amplitude of collected events used as parameter to distinguish between SCC and other corrosion processes Energy relaxation events because of SCC are considered much larger than energy release events during localized corrosion Principle Component Analysis (PCA) and K-mean clustering are used to classify signals Scanning electron microscopy (SEM) analysis revealed crack propagation by transgranular mode The crack initially propagates in mode I (shear cracking-like mechanism) and transitions to mode II (cleavage-like mechanism) after a certain subcritical growth

Table 3.2. (cont'd)

Reference/Purpose	Material	Notes/Results
(Yuyama et al. 1984) Study of corrosion fatigue in 304 stainless steel under using AE monitoring to determine applicability in BWR plants	304 stainless steel	<ul style="list-style-type: none"> • Sources of AE include: <ul style="list-style-type: none"> ◆ Crack initiation and growth ◆ Evolution of hydrogen gas via cathodic reactions ◆ Breakdown of thick oxide films • Crack tip plastic zone results in AE from: <ul style="list-style-type: none"> ◆ Martensitic transformation ◆ Slip deformation ◆ Twinning ◆ Fracture or decohesion of precipitates, second phase particles or non-metallic inclusions ◆ Microcracking • The AE energy rate under the corrosive environment is one order of magnitude higher than in-air or positive applied potential for equal macroscopic crack growth rate • AE in non-corrosive environment for solution treated specimens is caused by the cleavage of (111) planes. The cleavage of about three planes results in one AE event. • The higher AE activity in corrosive environments is attributed to separations caused by triaxial stress and hydrogen trapped at nonmetallic inclusions for solution-treated specimens (TGSCC) • Nucleation of separation is main source of AE during cracking of sensitized specimens • Higher AE activity is expected under plane strain than plane stress conditions because the effective yield stress under plane-strain conditions is much higher as a result of the plastic constraint • Sources that can provide high AE activity include cleavage-like cracking, intergranular cracking, or separations in the plane strain plastic zone ahead of the growing crack
(Jones and Freisel 1992) AE monitoring of pitting and transgranular crack initiation in Type 304 stainless steel	304 Stainless Steel	<ul style="list-style-type: none"> • IGSCC cracks on the order of 200 μm length and 100 μm deep could be detected using acoustic emission • Evidence of multiple stages in AE event emission versus time observed for samples exposed to mechanical stress and corrosive conditions • Rupture of thick oxide films covering pits suspected of being dominant source of AE

Table 3.3. Summary of Studies Involving the Use of AE to Degradation Phenomena at High Temperatures

Reference/Purpose	Material	Notes/Results
(Clark et al. 1982) AE monitoring of creep rupture in the HAZs of low alloy steels up to 690°C	CrMoV steels	<ul style="list-style-type: none"> • 3 different types of welds were monitored in CrMoV steels • Signals from creep failure are low amplitude; require the use of highly sensitive resonant transducers such as PZT 5A • Waveguides are used in this study • Noise due to oxide spalling may drown out cracking signals • Curing of the Berkatekt 29 coating meant to prevent oxide spalling is a source of AE below 550°C • Microstructure of samples has significant influence on how AE is generated until rupture. Regions of fine microstructure tend to arrest cracking resulting in an initial burst of AE followed by a dormant period followed by another burst of AE prior to creep rupture. Samples containing only coarse microstructure generated negligible AE until just before creep rupture. • Crack growth is rapid in coarse grained regions • The extent of damage measured by the crack surface area is related to AE activity • At high stresses, fine microstructures are not as effective at arresting cracks. At lower stresses, refined microstructures delay crack propagation and failure more effectively. • Is noted that transducer coupling and waveguide attachment welds contribute to test-to-test variability • Ringdown counts associated with fracture events range from 200 to 1000
(Clark 1979) Effort to find an appropriate coating to prevent oxidation during study of reheat cracking of CrMoV steels to temps of 690°C under stress using acoustic emission	CrMoV steels	<ul style="list-style-type: none"> • Coatings applied to test specimens in an effort to prevent oxidation which is recognized as a serious source of spurious AE signals • Resonant frequency transducers at 175 kHz and 750 kHz used for this study • DAG 2102 and Deltaglaze 47 and emulsion paint were not able to prevent oxidation completely • Snopake coating prevented oxidation but was a major source of AE itself • Berkatekt 29 and Berkstop N.T. prevented the oxidation and were quiet – thus considered the most ideal coatings for this study

Table 3.3. (cont'd)

Reference/Purpose	Material	Notes/Results
(Ferrer et al. 2001)	Alloy 800H	<ul style="list-style-type: none"> Monitoring up to 650°C Metal dusting described as a significant process in thermal cracking or ammonia plant environments Metal dusting develops uniformly for carbon steels and low alloy steels but for stainless steels and nickel-based alloys, it grows by pitting. AE waveguides attached to the inlet and outlet of the metal sample tube with wideband sensors Metal sample is UNS N08810 (alloy 800H) known to be very sensitive to metal dusting Waveguide attenuation determined to be about 10 dB (ASTM E 976) Metal dusting is characterized by an incubation period during which no AE is detected. After activation, AE activity displays linear relationship to damage progression Coking in the tube caused AE activity to cease Is postulated that coking process could be detected with AE if the detection threshold is decreased Breaking of oxide scales is often assumed responsible for ultrasonic wave generation associated with high temperature corrosion phenomena
(Ropital et al. 2004)	Ni, α -Fe, γ -Fe, Co, V, Mo, and Cr	<ul style="list-style-type: none"> Formation of carbon filaments in the temperature ranges of 450°C–700°C is a major problem in many chemical and petrochemical processes where hydrocarbons or other carburizing atmospheres are involved
Study the effectiveness of hydrogen sulfide as a coke deposition inhibitor using AE and thermogravimetric analysis (TGA)	Mo, and Cr metals	<ul style="list-style-type: none"> Coke formation involves reactions at the gas/metal interface and carbon diffusion within the metal Experiments performed on the following metals – Ni, α-Fe, γ-Fe, Co, V, Mo, and Cr. In carburizing and reducing atmospheres, reactions induce fragmentation of the oxide scale and the formation of graphite on the iron surface. Deposition of coke can be inhibited by selection of appropriate metallurgy, protection of surfaces by application of coatings, and injections of additives. Sulfur additives are commonly used in the industry Custom small size AE transducer with 300-kHz resonance attached to suspension quartz filament to remove from high temperature

Table 3.3. (cont'd)

Reference/Purpose	Material	Notes/Results
(Walter et al. 1993) Study of oxidation during thermal cycling of Alloy 800H and HK 40 in the chemical and petrochemical industries	Alloy 800H and HK 40 steels	<ul style="list-style-type: none"> • Noted that the oxide scales perform a protective function and damage is studied via acoustic emission • Isothermal tests on the alloy 800H were performed at 900°C and thermal cycling between 900°C and 100°C in several environments. Isothermal testing of HK 40 was conducted at 950°C along with thermal cycling between 950°C and 200°C in several environments. • For the alloy 800H sample, after large temperature drops, scale cracking events of large amplitude dominate. Most of the acoustic emission activity appears in between 200°C and 110°C. Considerable AE is generated upon heating the tube back up to 900°C. • For HK 40, maximum acoustic emission observed below 300°C with significant AE present on reheating • HK-40 generates more AE than Alloy 800H • Geometrically induced growth strains are of negligible magnitude compared with the thermally-induced strains from cooling
(Schmutzler and Grabke 1993) Study of oxidation layer damage under isothermal and thermal cycling conditions for high temperature alloys	Fe-18Cr-12Al and Fe-20Cr-5Al	<ul style="list-style-type: none"> • Oxide layers form on the surface of high temperature alloys containing sufficient Al or Cr to form a protective coating separating the metal from aggressive gas atmospheres • Oxide-metal composite is exposed to mechanical stresses during thermal cycling as a result of 1) thermal expansion mismatch of oxide and metal, 2) growth stresses due to oxide growth during isothermal oxidation • If the oxide layer is thin compared to the thickness of the metallic substrate, the elastic energy is stored mostly in the oxide scale • Sample is fixed to a Pt wire (1 mm in diameter) by spot welding. The Pt wire is connected to a piezoelectric sensor by two Au wires (0.125 mm in diameter). • Some AE signals detected above the background noise during isothermal oxidation • Acoustic-emission analysis is more sensitive in detecting oxide failures than thermogravimetric analysis. • The development of compressive stresses in the oxide layer during isothermal and thermal-cycling oxidation does not result in buckling of the scale but the formation of through-scale cracks and spallation of the scale. • The appearance of AE signals during isothermal oxidation of undoped Fe-18Cr-12Al is explained by repeated cracking and/or spalling of the α-Al₂O₃ layer. • Isothermal oxidation of undoped Fe-20Cr-5Al at 1273K produced very little AE activity but pronounced AE activity increasing with oxidation time was observed for undoped Fe-18Cr-12Al. AE signals attributed to buckling of the fine grain alumina layer formed on the Fe-20Cr-5Al and to repeated cracking and exfoliation of the coarse-grain alumina layer formed on Fe-18Cr-12Al. No AE signals were detected for Ce- and Y-doped Fe-Cr-Al alloys. • Thermal cycling of undoped Fe-20Cr-5Al led to a high number of AE signals in the first thermal cycle, and mass loss due to spallation of the oxide was observed at the third thermal cycle. Application of one thermal cycle to undoped Fe-18Cr-12Al caused a high number of acoustic-emission signals which resulted from oxide layer spallation.

Table 3.3. (cont'd)

Reference/Purpose	Material	Notes/Results
(Bennett et al. 1989)	20Cr-25Ni-Nb stainless steel	<ul style="list-style-type: none"> Uniform oxide scale forms on 20Cr-25Ni-Nb stainless steel when exposed to carbon dioxide-based environments between 750°C and 1000°C
Study of oxidation layer damage under isothermal and thermal cycling conditions for 20Cr-25Ni-Nb stainless steel	steel	<ul style="list-style-type: none"> Thin-layer activation (TLA) revealed that oxide spalling did not occur during isothermal exposure but did upon cooling Specimen attached to a 2.5 MHz damped acoustic transducer through an 0.92 mm diameter platinum wire acting as a waveguide and suspended in a silica reaction vessel In a second experimental arrangement, a sample and AE system were coupled with a controlled atmosphere microbalance system. The specimen was spot welded to a Pt-Rh alloy wire (0.64 mm in diameter) which was also the waveguide. The end of the Pt-Rh alloy wire was swan-neck shaped to minimize attenuation of the acoustic signals and was joined to a gold wire (0.13 mm in diameter) which was connected to the transducer AE system was calibrated using a known standard source of ultrasound – a Nd-YAG pulsed laser which produced a 10 ns, 12mJ pulse of 1.06 μm infrared light 20Cr-25Ni-Nb stainless steel was oxidized in carbon dioxide at 850°C, 950°C, or 1000°C from 5 to over 300 hrs. No AE was observed during isothermal exposure indicating no cracking or spalling of oxide scale. AE was observed upon cooling. A minimum scale weight was observed below which spallation could not be initiated at ambient temperature Above this threshold, the temperature required to initiate spallation decreased with increasing scale weight. This is consistent with thermal expansion differences between scale and metal being the primary source of stress generation. It was established in this study that scale cracking preceded spallation

Table 3.4. Summary of Several Piezoelectric Materials and Their Properties (Griffin et al. 2009)

Material	Frequency Constants, mm/MHz	Dielectric Constants	d_{33} Coefficient, m/V (-12)	G_{33} Coefficient, Vm/N (-3)	Coupling Factor, k_{33} (%)	Maximum Temperature, Degrees C	Mechanical, Q	K_p Planar Coupling Coefficient	Acoustic Impedance, gm/cm ² s
Quartz	2.87	4.5	2	50	11	550	10,000	---	15
Lithium Niobate, Y-Cut	3.68	30	6	23	15	1000	---	---	32
PZT-4	2.0	1300	15.5	26	70	328	500	0.58	30
PZT-5A	1.88	1700	375	25	70	365	75	0.6	29
Lead Zirconate Titanate									
K-81	1.65	300	85	32	40	400	15	0.1	20
Lead Niobate									
K-12	2.25	145	12	9.5	12	820	200	0.07	28.5
Bismuth Titanate									
K-15	2.0	130	18	10		600	100		≤29
Bismuth Titanate									
Tourmaline Z-Cut	7.1		1.8			1800			
Nova 3B	2.18	215	80	55	51	350	40	0.01	33

3.2.3 Localization Algorithms

AE generated by the formation of flaws and other defects consists of pulses that are clearly separated in time. Therefore, time-of-flight analysis can be applied to determine the location of a flaw generating AE. The time at which the AE event occurred is unknown, therefore, time-of-flight analysis is based on the relative arrival times of AE signals to individual sensors in an array. Multiple regression algorithms incorporated in commercial systems can locate the source of AE signals relative to the sensor array configuration (see Figure 3.2). Multiple regression algorithms determine the source location through a comparison of observed arrival times and calculated arrival times based on assumed source locations. This technique is an iterative process involving updates to the assumed source location in an effort to minimize the difference between calculated and observed arrival data (PAC 2005). Source locating algorithms assume signals have a well-defined velocity and that signals travel in straight lines. This limits the accuracy of locating AE sources since mode and material variation is unaccounted for. In addition, AE can originate from anywhere within a 3D structure or component whereas source locating algorithms only determine the coordinates in the 2D plane of the sensor array. Article 13, Section V of the ASME Code specifies that the source location accuracy of an AE array must be within one wall-thickness at the AE source location or 5% of the minimum sensor array spacing, whichever is greater.

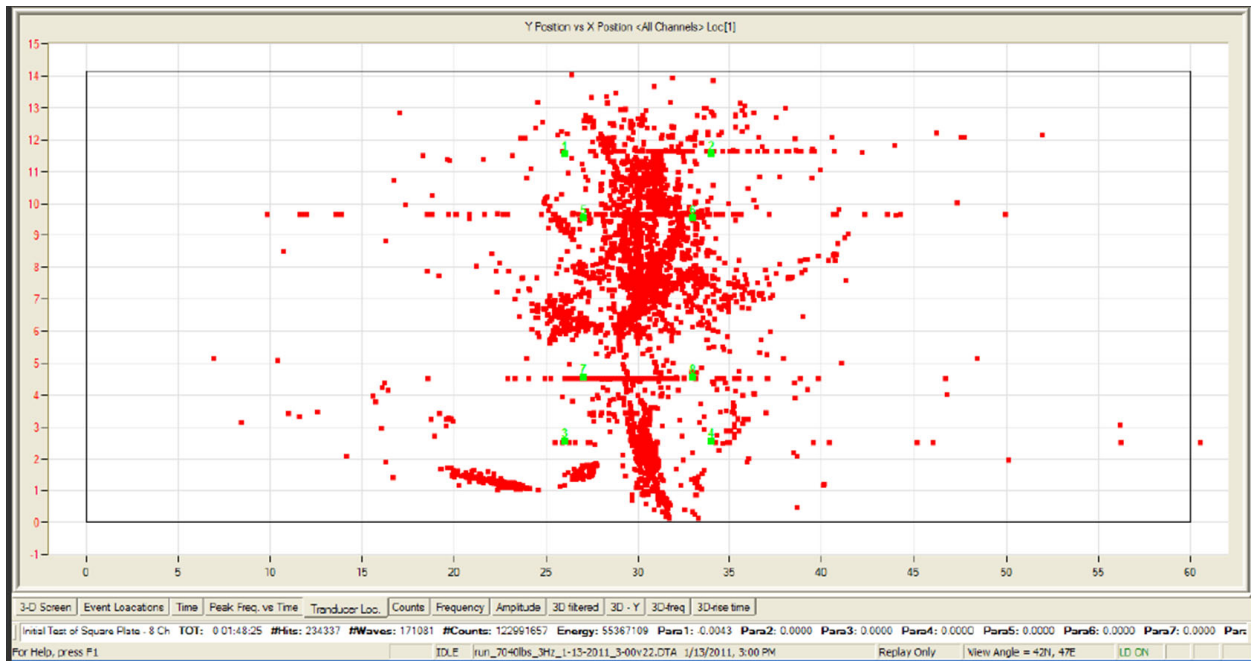


Figure 3.2. Screen Shot Obtained from a Commercial AE System Displaying the Location of AE Events Calculated Using a Multiple Regression Algorithm. The red dots indicate the location of AE events relative to the sensor array. The eight sensors are light green in color.

3.2.4 Signal Processing and Analysis

Modern AE systems include digital processors to extract signal features and software to visualize patterns among collected data. This facilitates the distinction between several groups of AE signals. An example of the data visualization capabilities is included in Figure 3.3. Specific signal features of interest with respect to signal interpretation and discrimination include (Pollock 2003):

- Amplitude (A)
- Measured area under rectified signal envelope (MARSE)
- Counts (N)
- Rise time (R)
- Duration (D)
- Energy (E)

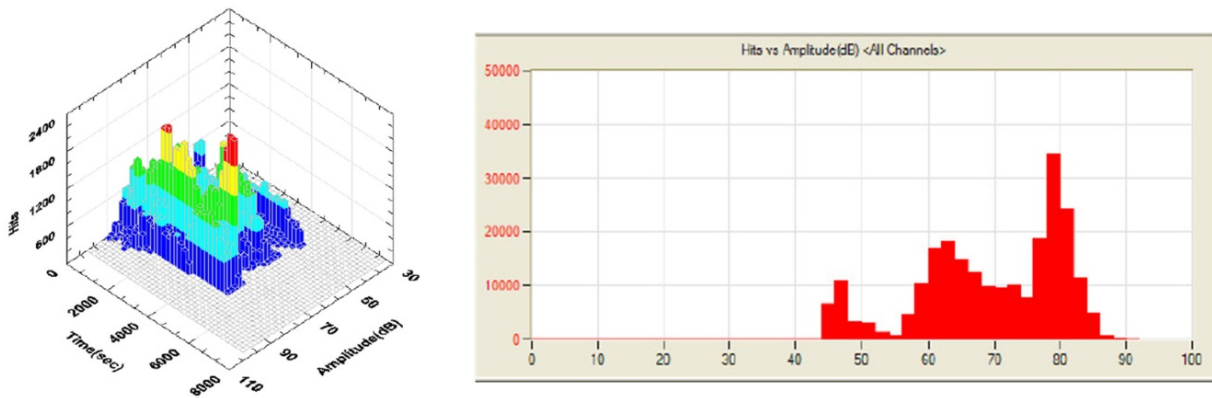


Figure 3.3. Example of Data Visualization Capabilities Provided Modern AE Systems Software

It should be noted that “Counts” refers to the total number of threshold crossings observed for a single AE waveform and that signal “Rise Time” and signal “Duration” are defined with respect to the initial and final threshold crossings. In addition to these time domain metrics, signal discrimination can be carried out on the basis of frequency spectrum characteristics.

Perhaps the simplest and most common means of signal discrimination is based on amplitude thresholding. AE signal processors normally include selectable input amplitude threshold settings to reject all signals below a certain amplitude associated with noise. This ensures resources are not wasted processing irrelevant signals.

Discrimination of AE signals based on amplitude distributions represents a common signal analysis strategy. The amplitude distributions of individual sources of AE are assumed to exhibit a power law shape described by (Sung et al. 1997):

$$F(V) = (V/V_{\text{thresh}})^{-b}. \quad (3.4)$$

$F(V)$ is a cumulative distribution function representing the probability that a signal amplitude exceeds V . V_{thresh} is selected such that $F(V_{\text{thresh}}) = 1$. This method is based on the assumption that different sources of AE will exhibit unique b-coefficient values.

The post-analysis of amplitude distributions along with patterns of other signal features is limited in effectiveness and/or subjective by nature. This has motivated attempts to develop improved algorithms for signal clustering and classification to automate the process in order to facilitate real-time analysis of signals and minimize measurement ambiguity. Techniques currently under investigation for clustering and classifying AE signals include K-means (Ramadan et al. 2008; Shaira et al. 2008), principle component analysis (Ramadan et al. 2008), and neural networks (Barga et al. 1990).

3.2.5 Calibration

The Hsu pencil source generates consistent signals via the breaking of pencil lead and can be used to test the reproducibility of an AE sensor response or the uniformity of many AE sensor responses. It is recommended to use 0.3 mm or 0.5 mm pencil lead with 2H level hardness. A “Nielson shoe” is a Teflon guide ring to aid in consistent breaking of pencil lead. Gas jets can be used to test AE sensor sensitivity and frequency response. Recommended test gases include helium or dry air with pressures between 150 kPa and 200 kPa (20 psi and 30 psi). Specific guidance for testing sensor sensitivity and response is included in Section V, Article 13 of the ASME Code. Instructions are provided regarding test gas, pressure, delivery and spacing between gas jet, AE sensor, and test block. Customized test signals can be introduced into a suitable test by use of a waveform generator and ultrasonic transducer. Specific guidance related to the selection of an ultrasonic transducer and the generation of acceptable signals is provided in ASTM E 976-98, “Standard Guide for Determining the Reproducibility of Acoustic Emission Sensor Response” (ASTM E 976 1998).

Automatic sensor testing (AST) functionality is incorporated in some commercial AE systems. These systems contain internal pulse generators to simulate AE waveforms. The simulated AE signal is introduced to the test component through one of the attached AE sensors. For an array of AE sensors, the response of nearby sensors to the AST provides a measure of sensitivity. The measured sensitivity can be impacted by any link in the AE instrumentation chain including: coupling layer at the interface of the AE sensor and component under test, AE sensor, pre-amplifier, and cable. AST also provides time-of-flight information among individual sensors in an AE sensor array which can be used to verify the functionality of location algorithms.

Laser energy sources can be used to calibrate AE sensors although laser techniques are not specified in the ASME Code. In the study by Bennett et al. (1989), the AE system was calibrated using a known standard source of ultrasound – a Nd-YAG pulsed laser, which produced a 10 ns, 12 mJ pulse of 1.06 μm infrared light.

ASTM E 976-98, “Standard Guide For Determining the Reproducibility of Acoustic Emission Sensor Response” (ASTM E 976 1998) describes specific test block designs to use in conjunction with performance testing of AE sensors. However, it is mentioned that design specificity is not so important as long as the test block is “non-resonant.”

3.2.6 Nuclear Power Applications

AE has been investigated as a means to detect leakage from primary pressure boundaries in LWRs. Leaks from cracks in primary reactor coolant boundaries result in the continuous generation of AE. For constant flow rates, it has been observed that the AE signals experience a decrease with decreasing temperature (Claytor and Kupperman 1985). A U.S. Nuclear Regulatory Commission (NRC)-sponsored laboratory study of AE for leak detection found that the estimated sensitivity of an AE leak monitoring system is strongly influenced by background noise, varying from 0.003 to 1.0 gpm depending on the noise level. Typically, leaks are detectable if the total AE signal is 3 dB above the background noise level. Sensors are usually attached through waveguides for leak monitoring in the vicinity of the reactor vessel (IAEA 2008). A significant conclusion of this study is that comprehensive leak monitoring of LWRs is feasible using AE requiring 135 sensors for a typical BWR and 105 sensors for a typical PWR. Further, maximum sensors spacings of 10 m, 2 m, and 1 m are calculated based on background noise levels of $4 \mu\text{V}_{\text{rms}}$, $20 \mu\text{V}_{\text{rms}}$, and $40 \mu\text{V}_{\text{rms}}$ (Kupperman et al. 2004).

AE has been used to detect loose parts within the primary coolant loop of nuclear steam system supplies. Loose part monitoring systems (LPMS) are used to detect and localize moving loose parts and estimate damage potential. Most PWRs have LPMSs and it is noted that these systems are most effective during reactor startup as most loose parts disintegrate or become lodged in the loop within the first 30 seconds after startup. Loose parts disintegrate by impact with other components, especially pump blades. Loose parts monitoring is usually implemented at audible and ultrasonic frequencies. Loose parts are usually identified as bursts in the time signal on top of the background noise level. Signal-to-noise ratio significantly impacts the effectiveness of loose parts monitoring and the false-alarm rate. In early systems, event recognition was mostly based on the analysis of signal amplitudes and the resulting false-alarm rates were high. More advanced systems incorporate sophisticated algorithms for loose parts recognition such as autoregressive modeling and Sequential Probability Ratio Test (SPRT), reducing false alarm rates below 1%. Work continues to compile a signature database of common events. Loose parts normally do not represent an immediate threat to the integrity of structural components; however, they can accelerate reactor aging. For instance, particulates from disintegrated loose parts can be carried into the reactor core and corrode the surface of fuel cladding (IAEA 2008).

AE has been deployed in the field to monitor the growth of cracks in two RPV nozzles at Limerick Generating Station Unit 1 (BWR) reactor and the Watts Bar Unit 1 (PWR) reactor. The flaws were known to exist and had first been characterized using conventional ultrasonic inspections. These tests demonstrated the ability of acoustic emission testing (AET) to discriminate AE signals due to crack growth from background noise caused by an active coolant loop and the ability to perform monitoring on components at temperatures near 300°C . AE was deployed for the duration of two fuel cycles at Limerick Unit 1 and operated well for the first fuel cycle. The equipment experienced degradation during the second fuel cycle as a result of thermal exposure (Hutton et al. 1993). A photograph of the Limerick Unit 1 nozzle and AE waveguide attachments is provided in Figure 3.4. These tests stemmed from more than two decades of work supported by the NRC and the U.S. Atomic Energy Commission.

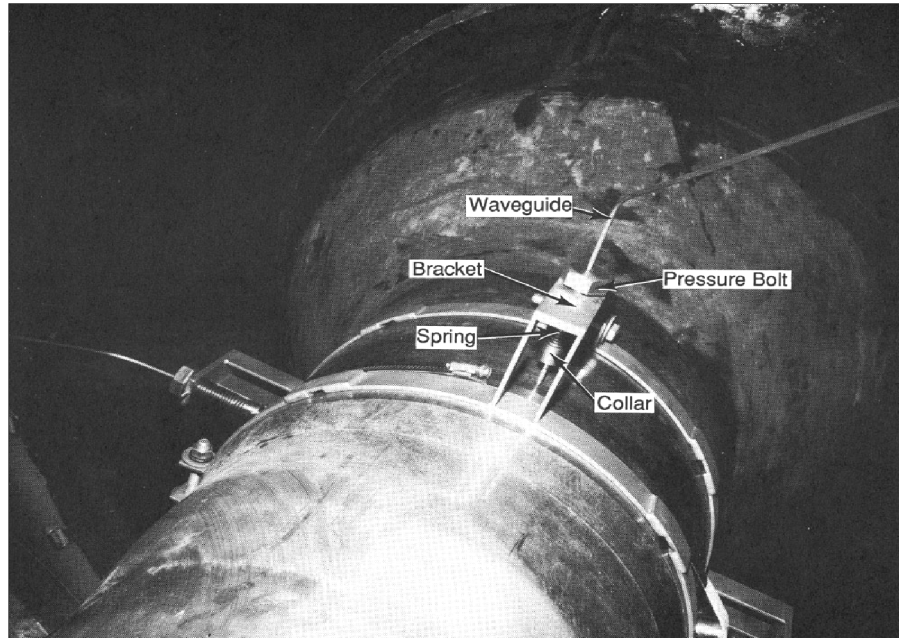


Figure 3.4. Photograph of AE Waveguide Attachment and RPV Nozzle at Limerick Unit 1 Reactor

An assessment of AE for application in Canada Deuterium-Uranium (CANDU) reactors was performed by Benz (1998). As part of this assessment, Benz considered the use of AE in several non-nuclear industries including the fossil power, chemical processing, compressed gas, and railroad industries. AE is commonly applied in hydrostatic and pressurization tests of vessel integrity. Additional applications of AE monitoring include leak monitoring, crack monitoring, and foreign/loose parts monitoring. Potential applications of AE monitoring in CANDU reactors identified from the assessment include valve leak monitoring, steam-line leak monitoring, and monitoring suspect areas for degradation. With regards to the state of acoustic emission monitoring in LWRs, Benz notes that AE is used extensively in the nuclear industry to detect leaks in valves and less extensively to detect leaks in piping (Benz 1998).

AE has been studied with respect to applications to liquid sodium cooled fast breeder reactors (LMFBRs). In particular, AE has been studied as a tool to detect the leaking of water into sodium in steam generators (Yugai et al. 1983; Pridoehl et al. 1984; Yugai and Sorokina 1986). Simulated leak studies were performed on a mock-up of a steam generator for the Superphenix reactor to assess AE sensitivity to these leaks. As part of this effort, sources of noise were characterized. Sodium flow noise was dominant below 2 kHz while the frequency range from 2 kHz–20 kHz was dominated by water/steam noise (Castelneau et al. 1980). Finally, it's noted that other LMFBR monitoring applications for AE include monitoring the cavitation of liquid sodium pumps, monitoring sodium boiling, and monitoring of structural vibrations (Burton 1976).

3.3 Acoustic Emission Codes and Standards

Use of acoustic emission for inservice inspection (ISI) of NPP SSCs is governed by Section XI of the ASME Code "Rules For Inservice Inspection of Nuclear Power Plant Components," Division I. The use

of acoustic emission for volumetric examinations is discussed in paragraph IWA-2234. Here, it is specified that AE may be used to monitor the growth of an existing flaw that has been characterized using another NDE technique. Evaluation of the growth rate based on AE measurements must be performed every two months and extrapolated to the next outage to determine if mitigating or repair activities are necessary or if operation can continue uninterrupted. Flaw growth is estimated from a relationship in Section V of the ASME Code, Article 13, Appendix I. This relationship is presented as Eq. 3.3 with $n - m = 0.53$ and $(C/(A^{n-m})) = 290$ and units of microinches/second for crack growth rate.

Generic requirements for continuous AE monitoring of pressure boundary components during operation are provided in Section V of the ASME Code, Article 13. Supplemental requirements for application of continuous AE monitoring of AE in NPPs is provided in Appendix I. Other supplemental requirements that are relevant to AE monitoring in NPPs are included in the following appendices:

- Appendix IV – “Limited Zone Monitoring”
- Appendix V – “Hostile Environment Applications”
- Appendix VI – “Leak Detection Applications”

Section V, Article 13 provides guidelines for sensor installation and calibration as well as requirements associated with other components of the AE monitoring system including cables, waveguides, preamplifiers, signal processor and data monitors. Generally, the current status of the code may not accurately reflect the state of modern AE technology since Article 13 was placed in the Code in the mid 1990s.

4.0 Guided Wave Monitoring

4.1 Background

Guided ultrasonic wave (GUW) monitoring is an active mode of monitoring as opposed to acoustic emission. GUW monitoring involves the introduction of energy into a component and observing reflections of that energy from flaws or other material discontinuities. GUW involves the introduction of ultrasonic waves with wavelengths on the same order of magnitude as the dimension of the component under inspection. As a consequence, boundary conditions significantly influence the propagation of GUW energy. In this scenario, the component under inspection supports the propagation of several GUW modes. Each of these modes experience dispersion that can result in significant variation of phase and group velocity (V_p and V_g , respectively) with respect to frequency. Brief descriptions of GUW propagation in plates and tubes will follow. More complete and rigorous discussions regarding GUW can be found in multiple texts (Rose 1999; Cheeke 2002).

4.1.1 Guided Waves in Plates

GUW propagation in plates is usually described using a Cartesian coordinate system. A plate of infinite extent in the x and y directions has a thickness b with surface normal vectors aligned with the z -axis. The sagittal plane is defined as the plane containing the surface normal vectors of the plate and the direction of wave propagation, defined in Figure 4.1 as the positive x -direction. GUWs polarized such that wave displacement is perpendicular to the sagittal plane are referred to as shear-horizontal (SH) waves (see Figure 4.1). Plates can support the propagation of many SH modes and the dispersion curves of the phase velocity for the first six SH modes are shown in Figure 4.2 for an aluminum plate. From Figure 4.2, it's clear that only the fundamental SH mode, SH₀, is supported at very low frequencies. Also, the figure indicates that the phase velocity for SH₀ remains fairly constant over the entire frequency range. Higher-order modes experience a frequency cutoff, below which their propagation in the plate is no longer supported. As the cutoff frequency of higher-order modes is approached from higher frequencies, a sharp increase in phase velocity is observed.

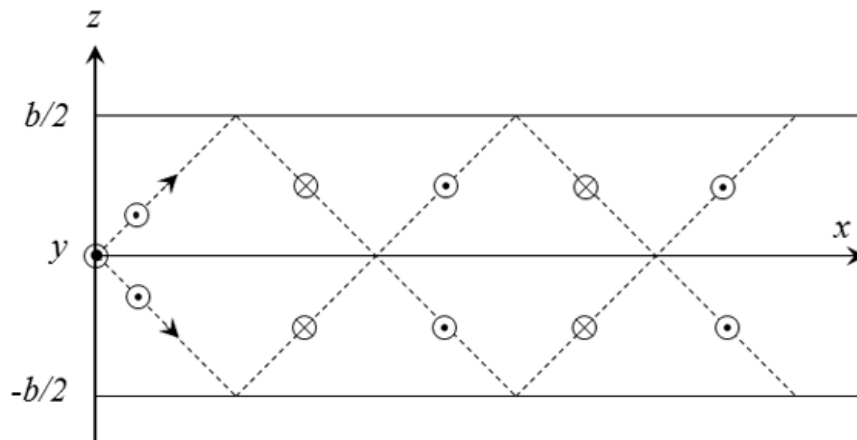


Figure 4.1. Vector Representation of SH Wave Propagation Along the x -direction of a Plate in the Sagittal Plane

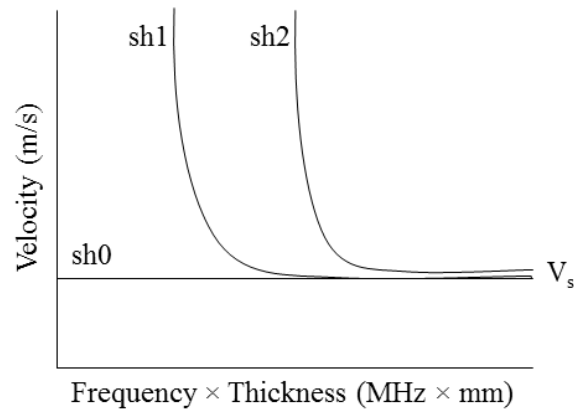


Figure 4.2. Dispersion Curves Calculated for the Phase Velocity of the First Three SH Modes in an Aluminum Plate

Lamb waves are polarized within the sagittal plane as shown in Figure 4.3. The propagation of several Lamb modes can be supported by a plate, and these modes are referred to as symmetric or antisymmetric modes referring to the variation in the displacement through the thickness of the plate. Dispersion curves for the phase velocity (solid lines) and group velocity (dashed lines) of the first six symmetric and antisymmetric modes are shown in Figure 4.4 for a brass plate. As with SH waves, it is clear that only the fundamental Lamb modes, A0 and S0, are supported at very low frequencies. Higher-order modes experience a frequency cutoff, below which, they cannot propagate.

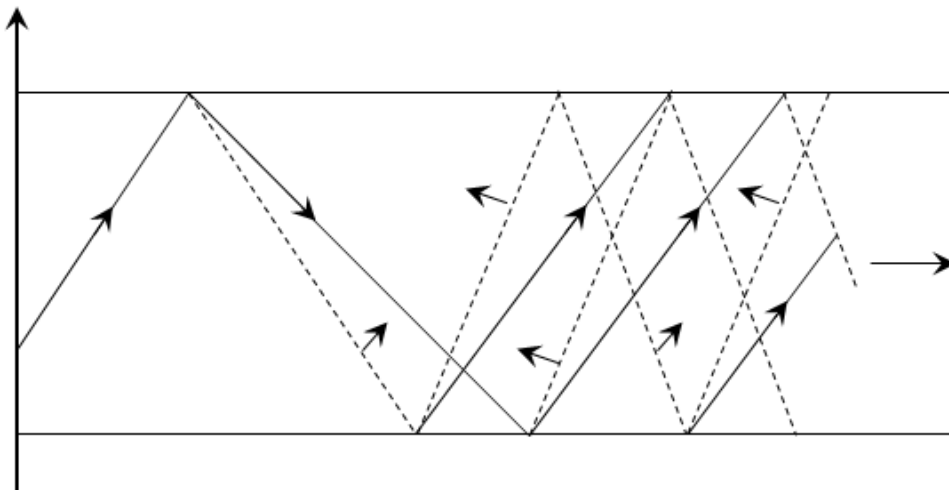


Figure 4.3. Vector Representation of Lamb Wave Propagation Along the x-direction of a Plate in the Sagittal Plane

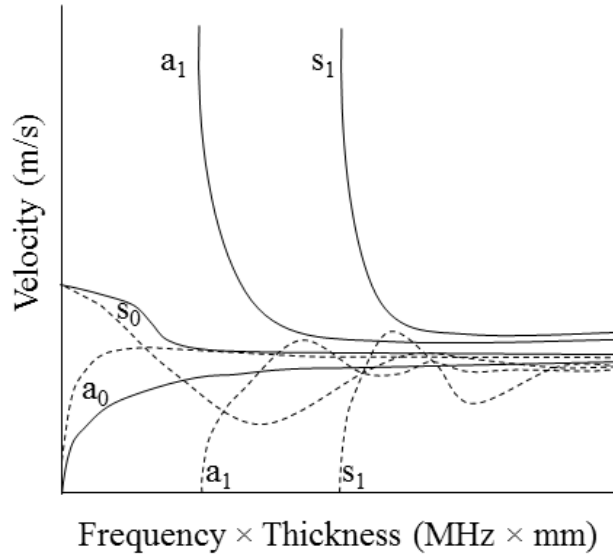


Figure 4.4. Dispersion Curves Calculated for the Phase and Group Velocities of the First Two Antisymmetric and Symmetric Modes in an Aluminum Plate

4.1.2 Guided Waves in Tubes

G UW propagation in tubes is best described in the cylindrical coordinate system with the axis of the cylinder aligned with the z -axis of the coordinate system, which also coincides with the direction of wave propagation. Waves can be polarized with displacements in the r , θ , and z directions referred to as flexural, torsional, and longitudinal waves. Illustration of longitudinal, flexural, and torsional mode excitation is provided in Figure 4.5 a)–c), respectively. The fundamental torsional mode experiences minimal attenuation in fluid-filled tubes making it an attractive mode for many pipe inspection applications such as the piping in LWRs or HTGRs. Pipe inspections are rarely performed based on flexural mode excitation.

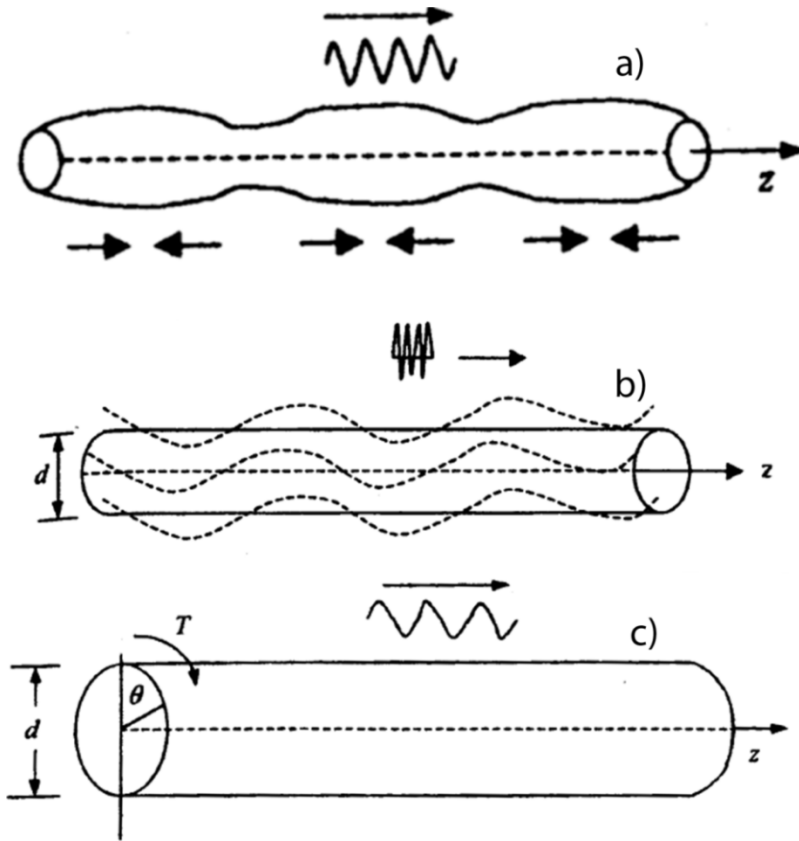


Figure 4.5. Illustration of a) Longitudinal Mode Excitation, b) Flexural Mode Excitation, and c) Torsional Mode Excitation in Tube-Shaped Structures (Rose 1999). Reprinted with the permission of Cambridge University Press.

4.2 GUV Sensors

Piezoelectric sensors for guided wave inspections may incorporate the same materials discussed in Section 3.2.1. Compared to the thickness vibration of a conventional bulk wave transducer, the piezoelectric transducer for guided wave application expands or contracts lengthwise. When placed in physical contact with the surface of a material under inspection, the lengthwise motion of the transducer transfers force to the material through friction and generates the guided wave. Detection of the guided wave is achieved by the reverse process (Naus 2007). Two common types of piezoelectric GUV transducers include the angle beam transducer and the comb transducer. The angle beam transducer shown in Figure 4.6 consists of a single piezoelectric element coupled to the test component through an acrylic shoe and ultrasonic coupling gel. Mode excitation is achieved through adjustment of the angle. The comb transducer shown in Figure 4.7 is a type of transducer used for pipe inspection. It includes an array of sensors distributed around the circumference of a pipe. Mode excitation in the comb transducer is achieved through sensor spacing. Excitation limited to a portion of the comb sensors results in the generation of nonaxisymmetric waves while excitation around the full circumference generates symmetric waves.

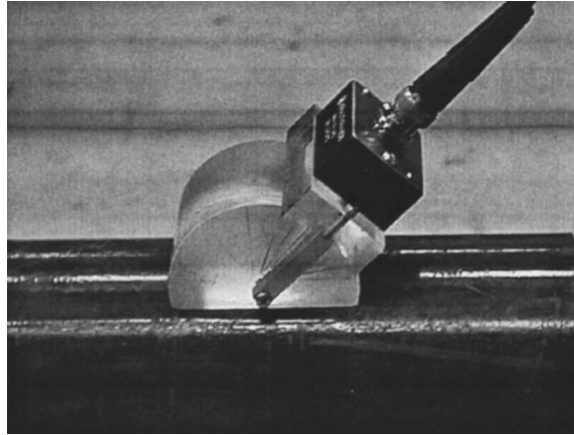


Figure 4.6. Photograph of an Angle Beam Transducer (Rose 2002). Reprinted by permission of ASME International.

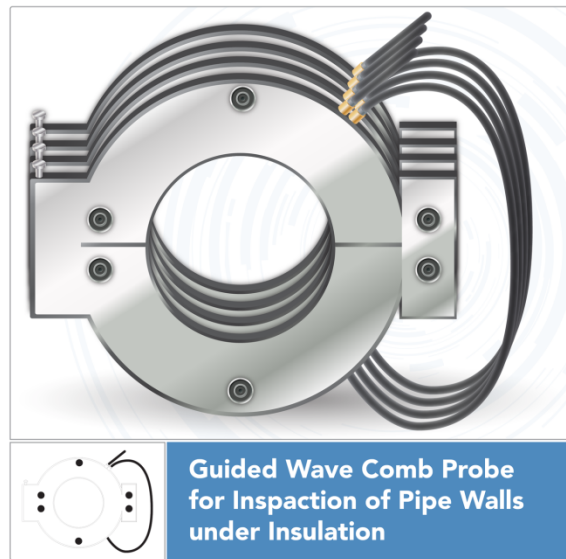


Figure 4.7. Drawing of a Comb Transducer

Magnetostrictive sensors (MsS) can transmit and receive guided waves in ferromagnetic materials to perform a flaw inspection. The MsS sensing mechanism is based on the force in ferromagnetic materials generated by strains associated with the motion of magnetic domains (Kittel 1949). The concept of MsS guided wave injection and detection is illustrated in Figure 4.8. The magnetic domains of the part under inspection are set into vibration by applying an alternating magnetic field to the part. Guided waves are then established as a result of the magnetic domain motion. The detection of guided waves with MsS follows from the reverse process where guided waves cause the magnetic domains in a material to vibrate. The motion of the magnetic domains caused the magnetic induction of the material to change. This change in magnetic induction induces a voltage in the MsS coil. The technique is contactless for ferromagnetic materials and is insensitive to surface conditions (Naus 2007). For other materials, MsS can induce guided waves with the aid of an intermediate strip of ferromagnetic material in direct contact

with the test component to convert magnetic domain motion to elastic wave motion. The range of guided wave inspections using MsSs can be on the order of 100 meters (Vinogradov and Kidd 2006).

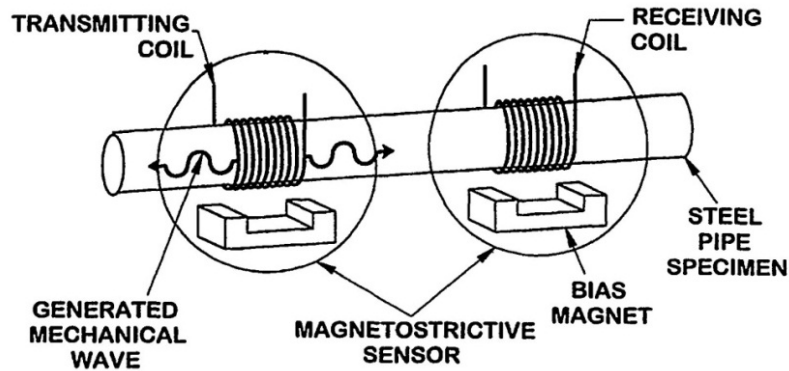


Figure 4.8. Illustration of MsS Guided Wave Injection and Detection Applied to a Steel Pipe (Kwun 1999). Reprinted with permission courtesy of Oak Ridge National Laboratory and the U.S. Nuclear Regulatory Commission.

Guided wave detection and generation is facilitated by the Lorentz force mechanism for electromagnetic acoustic transducers (EMATs). The Lorentz force is the force experienced by a moving charge in a static magnetic field (Krautkrämer and Krautkrämer 1990, Ch. 8). The EMAT contains a transmitter and a receiver (see Figure 4.9). Both components consist of a permanent magnet or electromagnet and a coil. The transmitter induces eddy currents in the test component through radio-frequency excitation. The induced eddy currents interact with the magnetic field from the coil to produce a Lorentz force and generate guided waves. Detection is achieved through the reverse process. EMATs are contactless transducers, are therefore insensitive to surface conditions, and can be applied through thin coatings of insulating material. Disadvantages of EMATs are that they are relatively inefficient and they are sensitive to the lift-off between the sensor and the surface of the test component (Naus 2007).

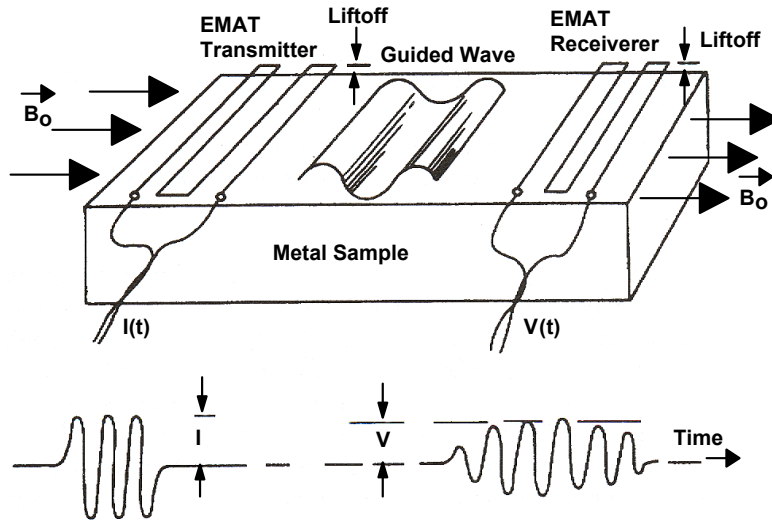


Figure 4.9. Illustration of EMAT Sensor for the Generation of Guided Ultrasonic Waves in a Metal Sample (Kwun 1999). Reprinted with permission courtesy of Oak Ridge National Laboratory and the U.S. Nuclear Regulatory Commission.

4.3 Nuclear Power Applications

The application of GUVs to structural monitoring is a relatively recent development. As a result, GUV technology is not widely deployed within the nuclear industry but recognition of its potential has been increasing. GUV signals are most easily interpreted when deployed on simple geometries such as tubes, rods, and plates and this is reflected by choice of components for which GUV has so far been applied. ASME Code Section V recently formed a task group to bring the GUV methodology into the code.

4.3.1 Containment Liners

GUV has been investigated for its ability to inspect difficult-to-access portions of metallic PWR containment structures or metallic plates lining the surface of BWR containment structures. Corrosion is a significant concern for containment structure metal that is embedded in concrete as moisture permeating the concrete can reach the embedded metal, which is difficult to access for inspection. EMATs have been used to launch SH_0 mode waves into a 25-mm steel plate representing a containment liner plate to investigate its ability to detect fabricated flaws. Flaws that were two wavelengths long and half through-thickness in depth were detectable from distances of several meters. It was observed that flaws with sharp features (such as a crack) produced stronger reflections than flaws with rounded features (such as corrosion) (Maxfield and Kuramoto 1988).

High frequency acoustic imaging of plate thinning caused by corrosion has been investigated numerically (Bondaryk et al. 1998) and experimentally (Rudzinsky et al. 1999) for free plates and plates embedded in concrete. Experimental studies were performed using angle-beam piezoelectric transducers tuned to 500 kHz to inject shear waves at multiple angles with respect to the surface of the plate. Degradation was simulated by fabricating several different notches into the surface of the plate. These

studies concluded that a rounded 4-mm-deep (25-mm plate thickness) flaw located 30 cm below the air/concrete interface should be detectable in the absence of competing signals. In addition, shallow angles of wave injection result in less attenuation for plates embedded in concrete (Rudzinsky et al. 1999).

Lamb waves have also been considered for the inspection of metallic liner plates that are free and backed by concrete on one or both sides. DISPERSE was used to calculate dispersion curves for the most fundamental modes, A₀, S₀, and S₁. DISPERSE is a commercial software tool for solving the wave equations and identifying the dispersion relations for a variety of waveguide structures and was developed at Imperial College beginning in 1990 (Imperial College). These simulations revealed little change in the group velocities for A₀ and S₀ modes between free plates and plates embedded in concrete. Further, minimal attenuation was observed for the A₀ modes below a frequency-thickness product of 0.55 MHz-mm. Experimentally, MsS probes were used to inject 20-kHz A₀ and 40-kHz S₀ modes into 6.35-mm-thick carbon steel plate. Fabricated notches and pits with lengths from 10 cm to 30 cm and depths of 50% through-thickness were studied. Under free-plate conditions, the A₀ mode experienced attenuation of 0.086 dB/m and the S₀ mode experienced attenuation of 0.33 dB/m (Kwun 1999). Covering the plate with concrete on one or both sides dramatically increased attenuation of S₀, A₀, and SH modes. It is concluded that S₀, SH, and high-frequency A₀ waves have limited inspection capability in concrete-covered areas (Kwun and Kim 2000).

4.3.2 Fuel Rod Cladding and Heat Exchanger Tubing

Torsional wave modes have been applied to detect simulated flaws in a fuel rod cladding mock-up. Torsional waves with a frequency of 250 kHz were selected to minimize the impact of grid spacers. Simulated corrosion pits, circumferential, axial, and 45° flaws were introduced to the zirconium alloy tube with the following dimensions: length – 3.91 m, diameter – 10.9 mm, wall thickness – 0.71 mm. The probe was capable of sampling the full length of the rod with the exception of a dead zone near the rod tip in the upper 30–40 cm of the fuel rod. The presence of grid spacers can interfere with small flaws located in regions near the spacers (Kwun et al. 2009). A diagram of the MsS probe configuration for inspection of fuel rod cladding is shown in Figure 4.10. MsS probes have also been applied to the inspection of U-bend areas in heat exchanger tubing. In this case, torsional guided wave modes at a frequency of 128 kHz were capable of detecting defects in the U-bend areas (Vinogradov and Kidd 2006). A photograph of the experimental setup for MsS inspection of heat exchanger tubing is including in Figure 4.11.

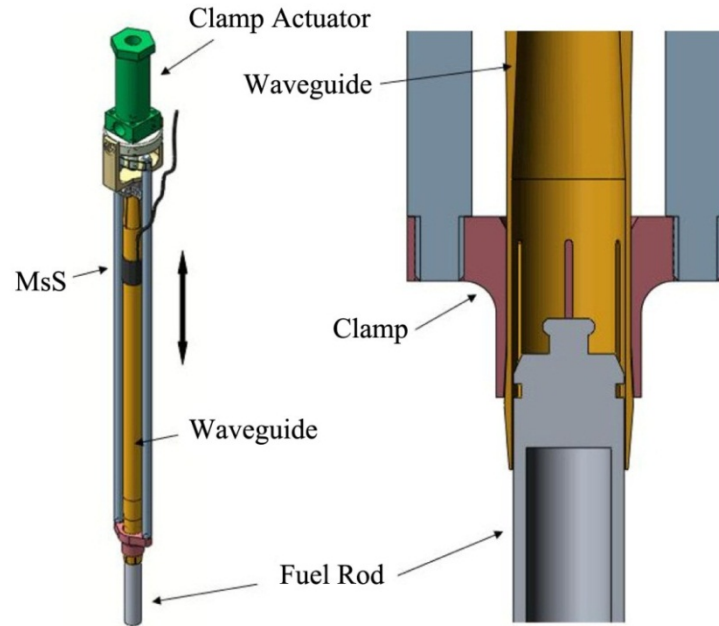


Figure 4.10. Illustration of MsS Applied to Guided Wave Inspection of Fuel Rod Cladding (Kwun et al. 2009). Image courtesy of Southwest Research Institute.

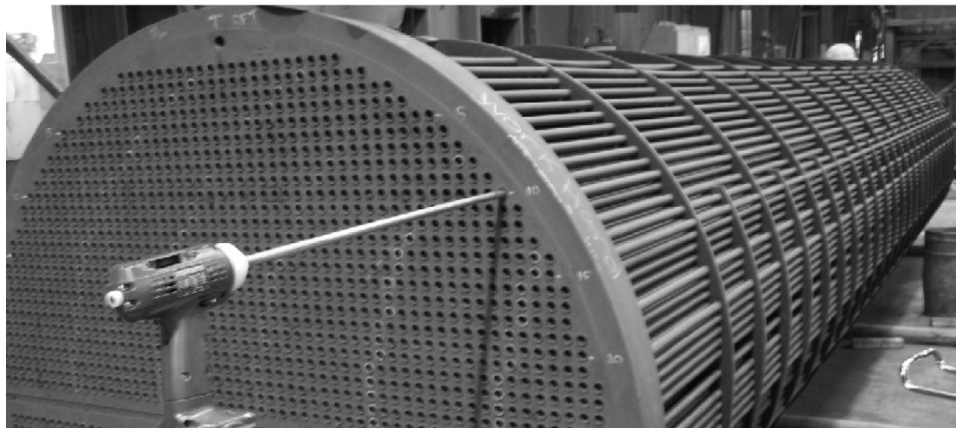


Figure 4.11. Application of MsS to Guided Wave Inspection of Heat Exchanger Tubing (Vinogradov and Kidd 2006). Reproduced with permission from Electric Power Research Institute, Palo Alto, California.

4.3.3 Underground Piping

GUWs have been investigated with respect to their ability to inspect underground or buried piping. Several different types of transducers have been investigated including angle beam, comb, EMATs, and MsSs (EPRI 2000). GUWs can detect wall thinning as a result of corrosion and other large defects. However, GUW is currently unable to inspect piping beyond joints or flanges and is unable to differentiate outer-diameter versus inner-diameter wall thinning. Flaw detection in underground and

buried piping must be followed up with more detailed assessments of flaw significance (EPRI 2008). A photograph of a comb transducer applied to the inspection of a pipe is included in Figure 4.12.



Figure 4.12. Application of a Comb Transducer to the Inspection of a Pipe (EPRI 2008). Reproduced with permission from Electric Power Research Institute, Palo Alto, California.

5.0 AE and HTGR – Discussion

5.1 Applications

Characterization of background noise in HTGR environments is important for assessing the efficacy of AE monitoring for several applications. Applications including leak detection, loose parts monitoring, and crack growth monitoring are all impacted negatively by high background noise levels. In addition, the efficacy of waveguide sensors is impacted by background noise levels. Coolant noise in LWRs has been attributed to cavitation, reactor coolant pumps, debris, and turbulent flows. Cavitation is not a factor in the operation of HTGRs; however, oxidation of high-temperature components may be a significant source of noise in HTGRs.

Limited zone monitoring is a potential application of AE in HTGR environments. Limited zone monitoring has been applied in LWR environments to monitor the growth of known flaws. AE could potentially be deployed in HTGRs to monitor suspect zones including welds, joints, and/or material discontinuities. Additionally, AE could potentially be deployed to monitor the growth of existing flaws. Background noise levels in HTGR environments could significantly influence the effectiveness of limited zone monitoring.

5.2 Sensitivity to Relevant Degradation Mechanisms

Aging and degradation mechanisms are usually classified into two main categories: 1) those that affect the internal microstructure or chemical composition of the material and thereby change its intrinsic properties (e.g., thermal aging, creep, irradiation damage), and 2) those that impose physical damage on the component either by metal loss (e.g., corrosion, wear) or by cracking or deformation (e.g., stress-corrosion, deformation, cracking). AE is typically more sensitive to the latter and confirmation of the sensitivity of AE to mechanical damage, corrosion, and SCC processes is extensively documented. The capability of AE monitoring for detecting fatigue cracking and SCC in ferritic steels, austenitic stainless steels and Ni-based alloys has been confirmed through extensive studies. Many of these studies are focused on detecting SCC crack growth in LWR environments. Little or no work has been done to evaluate the capability of AE to monitor SCC growth processes (radiation-assisted IGSCC) in austenitic stainless steels and Ni-based alloys in HTGR environments.

The sensitivity of AE to corrosion processes in LWR environments is documented in many AE studies of SCC for both austenitic stainless steels and Ni-based alloys. AE monitoring of corrosion processes at high temperature in carburizing atmospheres has been studied for applications in the fossil and chemical/petrochemical process industries. AE has been shown to be sensitive to carburization and coke deposition processes of stainless steels and Ni-based alloys at temperatures below 700°C. However, investigations of the application of AE to monitor similar processes in stainless steels and Ni-based alloys in HTGR environments are lacking. Few, if any studies address the application of AE to monitor decarburization in high temperature or HTGR environments.

AE monitoring is sensitive to oxidation processes. AE is sensitive to thick oxide layers that spall and crack. Most significant AE from oxide layers have been observed during thermal cycling in laboratory studies. However, significant AE may occur as a result of isothermal growth processes. Oxide scales

may be a significant source of noise in high-temperature components during normal operations and especially during shutdown of HTGRs.

Few studies address the application of AE to monitor creep effects. AE has been used to monitor creep rupture in the heat affected zone in a weld of CrMoV metal up to 690°C. Studies addressing the use of AE to monitor creep effects in austenitic stainless steels and Ni-based alloys are limited.

AE is sensitive to certain phase transformations, especially martensitic formation in austenitic stainless steels at low temperatures. Phase stability and radiation-induced segregation could be an issue for ferritic/martensitic steels, austenitic stainless steels, and Ni-based alloys. The sensitivity of AE to these phenomena has not been investigated.

Thermal fatigue could be a significant aging phenomenon in HTGRs and can lead to cracking. Few studies, if any, address the efficacy of AE for monitoring thermal fatigue effects.

Finally, several materials are under consideration for internal RPV structural components in addition to austenitic stainless steels and Ni-based alloys. These materials include graphite, ceramics, and composite materials. Literature related to the application of AE to monitor damage processes in these materials is limited.

5.3 Environmental Considerations and Waveguides

Life-time neutron fluences at RPV boundaries of HTGR RPVs will be near life-limiting neutron fluence levels for lead zirconate titanate (PZT) materials. AE has been deployed to monitor flaws in RPV nozzles of both PWR and BWR reactors. AE was deployed for two fuel cycles at the Limerick Unit 1 reactor and performed well for the first fuel cycle. System performance degraded in the second fuel cycle as a result of thermal exposure. Sensitive sensor components (piezoelectric transducers) were isolated from harsh temperature and neutrons in the immediate vicinity of the nozzle by attachment to a waveguide (2.75-m length). RPV temperatures of HTGRs (up to 370°C for cold barrels; up to 500°C for warm barrels) will be significantly higher than for LWRs (near 300°C). This implies a larger standoff distance is required for piezoelectric elements, increasing the necessary length of waveguides, which may reduce sensitivity. On the other hand, a new approach could be to use a cooling jacket for piezoelectric elements to limit the waveguides to a reasonable length. Alternatively, the development and use of AE sensors employing high-temperature piezoelectric elements could also mitigate excessive waveguide length. However, as highlighted in Table 3.4, there is normally a trade-off between the thermal tolerance of piezoelectric materials and their sensitivity.

AE waveguide sensors have been successfully deployed in laboratory testing above 900°C. Therefore, monitoring HTGR RPV internal components using waveguide sensors is conceivable. However, experience is lacking in using AE waveguide sensors as they have not been deployed to monitor LWR RPV internals. Some issues with monitoring RPV internals include signal attenuation in long waveguides and RPV penetration. Long-term reliability of the AE components at the elevated temperatures experienced in HTGRs will also need to be established.

5.4 Code Requirements

Section V and Section XI ASME Code requirements for AE testing are applicable to LWR monitoring. An equivalent set of requirements has not been developed for HTGRs. AE monitoring of LWRs is limited by Code requirements to crack growth monitoring and leak detection. Alternative NDE methods are relied upon for initial crack detection and accurate sizing of flaws. In practice, these functions are usually accomplished by periodic NDE during plant shutdown employing Appendix VIII qualified personnel, equipment, and procedures. In LWRs, AE monitoring supplements periodic NDE while in HTGRs, AE will replace periodic NDE implying that either AE or other online NDE methods will be relied upon for initial crack detection and accurate flaw size assessments. Current ASME Code rules also specify methods of sensor calibration and functional verification that must be performed offline. Finally, ASME Code requirements for AE monitoring may not be adequate to ensure inspections via AE monitoring are equivalent to inspections via periodic NDE.

5.5 G UW Monitoring

G UW monitoring is a promising technology for application to HTGRs and is currently seeing increased application in LWR structures and components. Liquid-filled pipes can attenuate G UW signals limiting the use of G UW monitoring for online applications in LWRs. The potential for online monitoring in HTGRs may be greater than LWRs because HTGRs are gas-cooled. The temperature of HTGR environments will be a limiting factor in the use of G UW sensors. However, the long-range inspection capability of G UWs may allow the inspection of components at high temperatures from a more tolerable environment.

6.0 Summary and Recommendations

AE can potentially be applied to many online monitoring (OLM) functions in HTGR environments. These functions include leak monitoring, loose parts monitoring, degradation monitoring, localized zone monitoring, and monitoring during pressurized testing of RPVs. The background noise in HTGRs is a source of uncertainty in predicting the efficacy of AE for the above OLM applications. While cavitation is described as a significant source of noise associated with LWR coolant loops, it will not be a factor in HTGRs. However, oxidation of components at high temperatures may introduce a significant source of noise in HTGRs that is not of consequence to the operation of LWRs. The high temperature of HTGR environments can also negatively impact the effectiveness and reliability of AE monitoring indirectly. Generally, the higher temperature environments in HTGRs relative to LWRs imply a larger standoff requirement for sensitive piezoelectric elements for many reactor components. Attenuation in waveguides is linearly related to waveguide length; thus, it is generally expected that AE sensors for HTGR applications will be less sensitive than waveguide sensors for LWR applications.

AE is most sensitive to gross physical damage in materials such as metal loss (corrosion, wear), cracking, and deformation. AE can potentially be deployed for local zone monitoring of degradation processes including corrosion, fatigue cracking, and SCC. In these cases, the monitoring zone may surround an existing flaw or may encompass a region of unusual stress concentration including welds and notches. The above degradation phenomena are common to both LWRs and HTGRs. Many degradation phenomena unique to HTGRs may be monitored with AE as well. Processes including oxidation, carburization, and creep rupture have all resulted in detectable AE in laboratory experiments employing waveguide sensors. More work is required to understand the capability of AE to monitor these processes in HTGR environments and in HTGR relevant environments

GUV monitoring is a promising technology with respect to HTGR monitoring. GUVs introduced to high-temperature structures will not be subject to attenuation by adjacent layers of liquids, potentially allowing for monitoring during HTGR operation. Additionally, the ability of GUV to monitor structures over a long range may allow for GUV monitoring of structures in harsh conditions from a more tolerable environment.

Recommendations for future R&D activities are based on the review of HTGR-relevant materials, degradation mechanisms, operating conditions, and the current state of AE and GUV monitoring technologies. Topics for future recommended activities include AE Code development for HTGR applications, AE sensor reliability, efficacy of AE leak detection and monitoring in HTGRs, AE sensitivity studies relevant to HTGRs, and GUV monitoring. The order in which the following recommendations are presented is not an indication of relative importance or priority.

The following are recommendations for future activities:

AE Code development for HTGRs

- Address what standards AE will have to meet in order to replace Section XI, Appendix VIII qualified personnel, equipment, and procedures.
- Devise standard methodologies for applying AE to monitoring of HTGRs.
- Qualify AE for detection of cracks and other forms of degradation in HTGR structural components.

- Qualify online methods of sensor calibration and functional verification.
- Develop criteria to quantitatively assess the size of leaks or extent of degradation using AE.
- Develop criteria to classify AE signals as signals from leaks versus signals from active degradation processes and other potential noise sources.

AE sensor reliability

- Evaluate alternative means of thermally shielding sensitive AE transducer components and electronics and active cooling methods in an effort to limit waveguide length and assess long-term reliability.
- Evaluate high-temperature AE transducers with respect to long-term reliability of monitoring applicable HTGR components.

Efficacy of AE leak detection and monitoring in HTGRs

- Obtain measurements of the AE noise level at relevant locations in an operating HTGR.
- Evaluate the ability of AE to detect He leakage in HTGR valves and piping. Determine minimally detectable leakage rates and effectiveness under operating conditions.

AE sensitivity studies relevant to HTGRs

- Assess the sensitivity of AE to fatigue and SCC cracking in ferritic steels at temperatures up to 370°C in a He environment.
- Assess the sensitivity of AE to fatigue, SCC cracking, creep, oxidation, and carburization in 9Cr-1Mo at temperatures up to 500°C in a He environment.
- Assess the sensitivity of AE to fatigue, SCC cracking, creep, oxidation, and carburization in austenitic stainless steels and Ni-based alloys at temperatures up to 950°C in a He environment.

GUV monitoring

- Demonstrate GUV inspection technologies on an active He loop and assess the impact of He on the ability of GUV to detect defects.

7.0 References

- Alvarez MG, P Lapitz and J Ruzzante. 2008. "AE Response of Type 304 Stainless Steel During Stress Corrosion Crack Propagation." *Corrosion Science* 50(12):3382-3388.
- ASME. 2010. *ASME Boiler and Pressure Vessel Code - An International Code, Section V Nondestructive Examination, Article 13 Continuous Acoustic Emission Monitoring, Mandatory Appendix V Hostile Environment Applications*. American Society of Mechanical Engineers, New York.
- ASNT. 2005. *Nondestructive Testing Handbook, Third Edition: Volume 6, Acoustic Emission Testing*. RK Miller, EvK Hill and PO Moore, American Society for Nondestructive Testing, Columbus, Ohio.
- ASTM E 976. 1998. *Standard Guide for Determining the Reproducibility of Acoustic Emission Sensor Response*. ASTM International, West Conshohocken, Pennsylvania.
- Ball SJ and SE Fisher. 2008. *Next Generation Nuclear Plant Phenomena Identification and Ranking Tables (PIRTs)*. NUREG/CR-6944, U.S. Nuclear Regulatory Commission, Washington, D.C.
- Barga RS, MA Friesel and RB Melton. 1990. "Classification of Acoustic-Emission Waveforms for Nondestructive Evaluation Using Neural Networks." In *Proceedings of SPIE, Volume 1294 - Application of Artificial Neural Networks*, pp. 545-556. April 16-20, 1990, Orlando, Florida. Society of Photo-Optical Instrumentation Engineers, Bellingham, Washington.
- Beech DJ and R May. 1999. "Gas Reactor and Associated Nuclear Experience in the UK Relevant to High Temperature Reactor Engineering." In *Survey on Basic Studies in the Field of High Temperature Engineering*. September 27-29, 1999, Paris. Nuclear Energy Agency, Organisation for Economic Co-operation and Development.
- Bennett MJ, DJ Buttle, PD Colledge, JB Price, CB Scruby and KA Stacey. 1989. "Spallation of Oxide Scales from 20%Cr---25%Ni---Nb Stainless Steel." *Materials Science and Engineering: A* 120-121(Part 1):199-206.
- Benz AEG. 1998. "Use of Acoustic Emission Techniques for Detection of Discontinuities [in CANDU reactors]." *Materials Evaluation* 56(10):1215-1222.
- Berkovits A and D Fang. 1995. "Study of Fatigue Crack Characteristics by Acoustic Emission." *Engineering Fracture Mechanics* 51(3):401-416.
- Bondaryk JE, CN Corrado and V Godino. 1998. *Feasibility of High Frequency Acoustic Imaging for Inspection of Containments*. NUREG/CR-6614, ORNL/SUB/97-SX754V, Oak Ridge National Laboratory, Oak Ridge, Tennessee.
- Buckthorpe D, R Couturier, B van der Schaaf, B Riou, H Rantala, R Moormann, F Alonso and B-C Friedrich. 2001a. "Investigation of High Temperature Reactor (HTR) Materials." In *Proceedings of the*

Second Information Exchange Meeting on Basic Studies in the Field of High-Temperature Engineering, pp. 203-213. October 10-12, 2001, Paris, France. NNC Ltd., Cheshire, United Kingdom.

Buckthorpe D, R Couturier, B van der Schaaf, B Riou, H Rantala, R Moormann, F Alonso and B-C Friedrich. 2001b. "Investigation of High Temperature Reactor (HTR) Materials." NNC Ltd., Cheshire, United Kingdom. Presented at 2nd Information Exchange Meeting on High Temperature Engineering, Paris, France, October 10-12, 2001.

Burton EJ. 1976. "The Development of Acoustic Monitoring Techniques for LMFBRs (In-Service Inspection and Monitoring of LMFBRs)." *Journal of the British Nuclear Energy Society* 15(3):265-270.

Castelnau L, T Desmas, F Mainy and A Lapicore. 1980. "In Service Monitoring and Servicing after Leak Detection for the LMFBR Steam Generators of Phenix and Superphenix." In *Special Topical Meeting - Materials Performance in Nuclear Steam Generators*. October 6, 1980, St. Petersburg Beach, Florida.

Chater J. 2005. "A History of Nuclear Power." *Focus on Nuclear Power Generation*:28-37.
http://www.focus-nuclear.com/pdf/TP_History_nuclear.pdf.

Cheeke JDN. 2002. *Fundamentals and Applications of Ultrasonic Waves*. CRC Press, Boca Raton, Florida.

Chen H-L and J-H Choi. 2004. "Acoustic Emission Study of Fatigue Cracks in Materials Used for AVL B." *Journal of Nondestructive Evaluation* 23(4):133-151.

Clark JN. 1979. "Surface Coatings to Prevent Oxidation during High Temperature Acoustic Emission Studies of Steel." *British Journal of Nondestructive Testing* 21(6):312-316.

Clark RA, GB Dudder and FL Becker. 1982. "Fabrication of Cracks for Ultrasonic Procedures and Personnel Qualifications." In *Quantitative NDE in the Nuclear Industry*, pp. 463-467. ed: RB Clough. PNL-SA-10459.

Clayton TN and DS Kupperman. 1985. "Characterization of Acoustic Emission Signals Generated by Water Flow Through Intergranular Stress Corrosion Cracks." In *International Conference on Acoustic Emission*, pp. 69-73. Lake Tahoe, Nevada. Acoustic Emission Working Group.

Corwin WR, R Ballinger, S Majumdar, KD Weaver and S Basu. 2008. *Next Generation Nuclear Plant Phenomena Identification and Ranking Tables (PIRTs), Volume 4: High-Temperature Materials PIRTs*. NUREG/CR-6944, Vol. 4; ORNL/TM-2007/147, Vol. 4, Oak Ridge National Laboratory, Oak Ridge, Tennessee.

Dukes R and EA Culpan. 1984. "Acoustic Emission: Its Techniques and Applications." *Physical Science, Measurement and Instrumentation, Management and Education - Reviews, IEE Proceedings A* 131(4):241-251.

- Dunegan HL, DO Harris and AS Tetelman. 1970. "Detection of Fatigue Crack Growth by Acoustic Emission Techniques." *Materials Evaluation* 28(10):221-227.
- EPRI. 2008. *Recommendations for an Effective Program to Control the Degradation of Buried Piping*. EPRI 1016456, Electric Power Research Institute (EPRI), Charlotte, North Carolina.
- Ferrer F, C Brun, J Goudiakas and E Andres. 2001. "Acoustic Emission Study of Dimethyl Disulfur as Metal Dusting Inhibitor." In *Corrosion 2001*. March 11-16, 2001, Houston, Texas. NACE International. Paper 01386.
- Griffin JW, TJ Peters, LJ Bond, KM Denslow, GJ Posakony, SH Sheen, P Raptis and HT Chien. 2009. *Under Sodium Viewing: A Review of Ultrasonic Imaging Technology for Liquid Metal Fast Reactors*. PNNL-18292, Pacific Northwest National Laboratory, Richland, Washington.
- Harris DO and HL Dunegan. 1974. "Continuous Monitoring of Fatigue-Crack Growth by Acoustic-Emission Techniques." *Experimental Mechanics* 14(2):71-81.
- Hutton PH. 1993. "Listening to Reactor Pressure Boundaries for the Sounds of Cracks and Leaks." *Nuclear Engineering International* 38(473):38-40.
- Hutton PH, JF Dawson, MA Friesel, JC Harris and RA Pappas. 1984. *Acoustic Emission Monitoring of Hot Functional Testing: Watts Bar Unit 1 Nuclear Reactor*. NUREG/CR-3693, PNL-5022, Nuclear Regulatory Commission, Washington, D.C.
- Hutton PH, MA Friesel and JF Dawson. 1993. *Continuous AE Crack Monitoring of a Dissimilar Metal Weldment at Limerick Unit 1*. NUREG/CR-5963, PNL-8844, U.S. Nuclear Regulatory Commission, Washington, D.C.
- IAEA. 1997. *Fuel Performance and Fission Product Behaviour in Gas Cooled Reactors*. IAEA-TECDOC-978, International Atomic Energy Agency, Vienna, Austria.
- IAEA. 2005. *Assessment and Management of Ageing of Major Nuclear Power Plant Components Important to Safety: BWR Pressure Vessels*. IAEA-TECDOC-1470, International Atomic Energy Agency, Vienna, Austria.
- IAEA. 2007. *Assessment and Management of Ageing of Major Nuclear Power Plant Components Important to Safety: PWR Pressure Vessels*. IAEA-TECDOC-1556, International Atomic Energy Agency, Vienna, Austria.
- IAEA. 2008. *On-line Monitoring for Improving Performance of Nuclear Power Plants, Part 2: Process and Component Condition Monitoring and Diagnostics*. IAEA Nuclear Energy Series No. NP-T-1.2, International Atomic Energy Agency (IAEA), Vienna, Austria.
- Imperial College. *Disperse Software*. Imperial College. London. Accessed December 5, 2011 Available at <http://www3.imperial.ac.uk/nde/products%20and%20services/disperse>.

- INL. 2010a. *HTGR Technology Course for the Nuclear Regulatory Commission, May 24-27, 2010, Module 11 - High Temperature Materials Performance*. Idaho National Laboratory (INL), Idaho Falls, Idaho.
- INL. 2010b. *NGNP High Temperature Materials White Paper*. INL/EXT-09-17187, Idaho National Laboratory (INL), Idaho Falls, Idaho.
- Jones RH and MA Freisel. 1992. "Acoustic Emission During Pitting and Transgranular Crack Initiation in Type 304 Stainless Steel." *Corrosion* 48(9):751-758.
- Jones RH, MA Friesel and R Pathania. 1991. "Evaluation of Stress Corrosion Crack Initiation Using Acoustic Emission." *Corrosion* 47(2):105-115.
- Kittel C. 1949. "Physical Theory of Ferromagnetic Domains." *Review of Modern Physics* 21(4):541-583.
- Krautkrämer J and H Krautkrämer. 1990. *Ultrasonic Testing of Materials, 4th fully revised Edition*. Springer-Verlag, New York.
- Kupitz J and JB Dee. 1984. "International Status of HTGRs." *IAEA Bulletin* 26(4):5-10.
- Kupperman DS, SH Sheen, WJ Shack and DR Diercks. 2004. *Barrier Integrity Research Program*. NUREG/CR-6861, ANL-04/26, U.S. Nuclear Regulatory Commission, Washington, D.C.
- Kwun H. 1999. *Feasibility of Magnetostrictive Sensor Inspection of Containments*. NUREG/CR-5724, ORNL/SUB/98-SZ272V, U.S. Nuclear Regulatory Commission, Washington, D.C.
- Kwun H and SY Kim. 2000. *Experimental Validation of Concrete Effects on Guided Waves in Plate*. EPRI Technical Report 1000105, Electric Power Research Institute, Charlotte, North Carolina.
- Kwun H, E Mader and K Krzywosz. 2009. "Guided Wave Inspection of Nuclear Fuel Rods." In *Proceedings of the 7th International Conference on NDE in Relation to Structural Integrity for Nuclear and Pressurised Components*. May 12-14, 2009, Yokohama, Japan. European Commission Joint Research Centre, Luxembourg.
- La Bar MP and WA Simon. 1997. "International Co-operation in Developing the GT-MHR." In *Proceedings of High Temperature Gas Cooled Reactor Technology Development*, pp. 59-72. November 13-15, 1996, Johannesburg, South Africa. International Atomic Energy Agency, Vienna, Austria. IAEA-TECDOC-988.
- Lecomte M. 1999. "Revised Version of HTR." In *Survey on Basic Studies in the Field of High Temperature Engineering*. September 27-29, 1999, Paris. Nuclear Energy Agency, Organisation for Economic Co-operation and Development.

Lenain J-C and A Proust. 2005. "Active Corrosion Detection Using Acoustic Emission." *Materials Evaluation* 63(10):1023-1030.

Maxfield BW and A Kuramoto. 1988. *The Feasibility of Using Electromagnetic Acoustic Transducers to Detect Corrosion in Mark I Containment Vessels*. EPRI NP-6090, Electric Power Research Institute, Palo Alto, California.

Moorthy V, T Jayakumar and B Raj. 1994. "Acoustic Emission Behavior During Stage II Fatigue Crack Growth in an AISI Type 316 Austenitic Stainless Steel." *Bulletin of Materials Science* 17(6):699-715.

Mukhopadhyay CK, T Jayakumar, B Raj and KK Ray. 2000. "Acoustic Emission--Stress Intensity Factor Relations for Tensile Deformation of Notched Specimens of AISI Type 304 Stainless Steel." *Materials Science and Engineering A* 293:137-145.

Mukhopadhyay CK, KK Ray, T Jayakumar and B Raj. 1998. "Acoustic Emission from Tensile Deformation of Unnotched and Notched Specimens of AISI Type 304 Stainless Steels." *Materials Science and Engineering A* A255(1-2):98-106.

Murty KL and I Charit. 2008. "Structural Materials for Gen-IV Nuclear Reactors: Challenges and Opportunities." *Journal of Nuclear Materials* 383(1-2):189-195.

Naus DJ. 2007. *Inspection of Nuclear Power Plant Structures – Overview of Methods and Related Applications*. ORNL/TM-2007/191, Oak Ridge National Laboratory, Oak Ridge, Tennessee.

O'Donnell WJ, AB Hull and S Malik. 2008. "Historical Context of Elevated Temperature Structural Integrity for Next Generation Plants: Regulatory Safety Issues in Structural Design Criteria of ASME Section III Subsection NH." In *ASME 2008 Pressure Vessels and Piping Conference (PVP2008)*, pp. 729-738 Chicago, Illinois.

PAC. 2005. *DiSP with AEwin, User's Manual, Rev. 3*. PAC Part #6320-1001, Physical Acoustics Corporation (PAC), A MISTRAS Holdings Company, Princeton Junction, New Jersey. Associated with AEwin Software, PAC Part #6320-7030, Version 1.90, or Higher.

Parks D and BR Tittmann. 2011. *Ultrasonic NDE in a Reactor Core*. Presented at Review of Progress in Quantitative NDE, July 17-22, 2011, Burlington, Vermont. Special Session: Acoustic Sensors for Extreme Environments. Paper 1077.

Pollock AA. 2003. *Acoustic Emission Inspection*. Technical Report TR-103-96-12/89, Physical Acoustics Corporation, Princeton Junction, New Jersey

Pridoehl E, H Mauersberger, D Hamann and G Hoehnel. 1984. "Surveillance of LMFBR Steam Generators by Acoustic Monitoring." In *Proceedings of the Third International Conference on Liquid Metal Engineering and Technology*, pp. 151-157. April 9-13, 1984, Oxford, England. British Nuclear Energy Society, London.

Ramadan S, L Gaillet, C Tessier and H Idrissi. 2008. "Assessment of the Stress Corrosion Cracking in a Chloride Medium of Cables Used in Prestressed Concrete Structures by the Acoustic Emission Technique." *Measurement Science & Technology* 19(11):115702 (9 pp.).
<http://dx.doi.org/10.1088/0957-0233/19/11/115702>.

Rogers LM. 2005. "Crack Detection Using Acoustic Emission Methods - Fundamentals and Applications." *Key Engineering Materials* 293-294:33-45.

Ropital F, P Dascotte, P Marchand, T Faure, JC Lenain and A Proust. 2004. "Coupling Thermogravimetric and Acoustic Emission Measurements: Its Application to Study the Inhibition of Catalytic Coke Deposition." In *EUROCORR 2004 - Long Term Prediction and Modeling of Corrosion*. September 12-16, 2004, Nice, France.

Rose JL. 1999. *Ultrasonic Waves in Solid Media*. Cambridge University Press, Cambridge, United Kingdom.

Rose JL. 2002. "A Baseline and Vision of Ultrasonic Guided Wave Inspection Potential." *Journal of Pressure Vessel Technology* 124:273-282.

Rudzinsky J, J Bondaryk and M Conti. 1999. *Feasibility of High Frequency Acoustic Imaging for Inspection of Containments: Phase II*. ORNL/NRC/LTR-99/11, Oak Ridge National Laboratory, Oak Ridge, Tennessee.

Schmutzler HJ and HJ Grabke. 1993. "Application of an Acoustic-Emission Technique to the High-Temperature Oxidation of Fe-Cr-Al Alloys." *Oxidation of Metals* 39(1/2):15-29.

Shaikh H, R Amirthalingam, T Anita, N Sivaibharasi, T Jaykumar, P Manohar and HS Khatak. 2007. "Evaluation of Stress Corrosion Cracking Phenomenon in an AISI Type 316LN Stainless Steel Using Acoustic Emission Technique." *Corrosion Science* 49(2):740-765.

Shaira M, N Godin, P Guy, L Vanel and J Courbon. 2008. "Evaluation of the Strain-Induced Martensitic Transformation by Acoustic Emission Monitoring in 304L Austenitic Stainless Steel: Identification of the AE Signature of the Martensitic Transformation and Power-Law Statistics." *Materials Science and Engineering A* 492:392-399.

Sinclair ACE, DC Connors and CL Formby. 1977. "Acoustic Emission Analysis During Fatigue Crack Growth in Steel." *Materials Science and Engineering* 28:263-273.

Sung KY, IS Kim and YK Yoon. 1997. "Characteristics of Acoustic Emission During Stress Corrosion Cracking of Inconel 600 Alloy." *Scripta Materialia* 37(8):1255-1262.

Verfondern K, H Nabielek and JM Kendall. 2007. "Coated Particular Fuel for High Temperature Gas Cooled Reactors." *Nuclear Engineering and Technology* 39(5):603-616.

Vinogradov S and G Kidd. 2006. "Advanced Guided Wave Piping and Tubing Inspection Using Magnetostrictive Sensor Technology." In *Fifth International Conference on NDE in Relation to*

Structural Integrity for Nuclear and Pressurised Components, May 10-12, 2006, San Diego, California.
eds: M Bieth and J Whittle. European Commission Joint Research Centre.

Walter M, M Schütze and A Rahmel. 1993. "Behavior of Oxide Scales on Alloy 800 H and HK 40 During Thermal Cycling." *Oxidation of Metals* 40(1):37-63.

Yugai VS, RF Masagutov and FA Kozlov. 1983. "Acoustic Effects from Water Leaking Into Sodium." *Soviet Atomic Energy* 54(3):173-177.

Yugai VS and TG Sorokina. 1986. "Acoustic Boiling Noise in a Sodium-Water Steam Generator." *Soviet Atomic Energy* 60(3):270-272.

Yuyama S, T Kishi and Y Hisamatsu. 1984. "Fundamental Aspects of AE Monitoring of Corrosion Fatigue Processes in Austenitic Stainless Steel." *Journal of Materials for Energy Systems* 5(4):212-221.

Zhang W, L Dunbar and D Tice. 2008. "Monitoring of Stress Corrosion Cracking of Sensitised 304H Stainless Steel in Nuclear Applications by Electrochemical Methods and Acoustic Emission." *Energy Materials: Materials Science and Engineering for Energy Systems* 3(2):59-71.



Pacific Northwest
NATIONAL LABORATORY

*Proudly Operated by **Battelle** Since 1965*

902 Battelle Boulevard
P.O. Box 999
Richland, WA 99352
1-888-375-PNNL (7665)
www.pnl.gov



U.S. DEPARTMENT OF
ENERGY